▌ Chemical Bonding

The Valence Orbitals of the Alkaline-Earth Atoms

Israel Fernández[+],*[a] Nicole Holzmann[+],[b] and Gernot Frenking*[c, d]

Dedicated to Professor Peter Schwerdtfeger on the occasion of his 65th birthday

Abstract: Quantum chemical calculations of the alkaline-earth oxides, imides and dihydrides of the alkaline-earth atoms (Ae = Be, Mg, Ca, Sr, Ba) and the calcium cluster $Ca_6H_9[N(SiMe_3)_2]_3(pmdta)_3$ (pmdta = N,N,N',N'',N''-pentamethyldiethylenetriamine) have been carried out by using density functional theory. Analysis of the electronic structures by charge and energy partitioning methods suggests that the valence orbitals of the lighter atoms Be and Mg are the (n)s and (n)p orbitals. In contrast, the valence orbitals of the heavier atoms Ca, Sr and Ba comprise the (n)s and $(n-1)$d orbitals. The alkaline-earth metals Be and Mg build covalent bonds like typical main-group elements, whereas Ca, Sr and Ba covalently bind like transition metals. The results not only shed new light on the covalent bonds of the heavier alkaline-earth metals, but are also very important for understanding and designing experimental studies.

Introduction

The alkaline-earth (Ae) metals of group 2 of the periodic table of elements traditionally belong to the class of main-group atoms and their valence electrons occupy the (n)s atomic orbital in the ^{1}S electronic ground state. The most common oxidation state of Ae atoms is $+2$, although molecules of Be and Mg with the formal oxidation states $+1$ and 0 are known and have been the topic of recent theoretical and experimental studies.[1] The heavier homologues Ca, Sr and Ba mainly occur as salt compounds in which the cations M^{2+} are stabilised by anions in the solid state or by polar solvents in solution. The rather low ionisation energies of the latter Ae elements foster the formation of ionic salts as the most common compounds of Ca, Sr and Ba.[2]

The dominant appearance of the heavier Ae elements Ca, Sr and Ba in salt compounds may be the reason why the covalent bonding of the atoms in molecular compounds has been less investigated in the past. The nature of the bonding in the solid state and in a molecule can be very different, which is evidenced by the equilibrium bond lengths in the two states. For example, the Ca—O distance in solid calcium oxide is 2.40 Å,[3] whereas the interatomic distance of diatomic CaO is only 1.821 Å.[4] The chemical bond in solid CaO may correctly be discussed in terms of ionic interactions between Ca^{2+} and O^{2-} species, for which lattice interactions provide a stable surrounding in the crystal state.[5] In contrast, the polar bond in diatomic CaO emanates from covalent interactions between the atoms due to the interference of the wave functions and also from electrostatic attractions between the resulting charge distributions, but not from ionic interactions. The latter type of bonding is only found between charged species with negligible orbital overlap in ionic crystals, which require lattice interactions between all ions to provide a stable system. Electrostatic attraction in polar and non-polar[6] covalent bonds stems from overlapping charge distribution. The physical misinterpretation of polar covalent bonds as partially ionic bonds goes back to the work of Pauling, who explained the quantum theoretical nature of the chemical bond by using solely valence bond (VB) theory.[7] In VB theory, only non-polar covalent bonds and ionic bonds are considered, with polar bonds being described by a mixture of these two types of bond. Identification of the VB with the physical nature of the chemical bond is misleading.

The present work focuses on the covalent bonding of the heavier alkaline-earth atoms in small molecules, which may serve as models for polar bonds in molecular compounds of

[a] Dr. I. Fernández[+]
Departamento de Química Orgánica I, and Centro de Innovación en Química Avanzada (ORFEO-CINQA), Facultad de Ciencias Químicas Universidad Complutense de Madrid, 28040 Madrid (Spain)
E-mail: israel@quim.ucm.es

[b] Dr. N. Holzmann[+]
Research Center for Computer-Aided Drug Discovery
Shenzhen Institutes of Advanced Technology
Chinese Academy of Sciences, Shenzhen 518055 (China)

[c] Prof. G. Frenking
Fachbereich Chemie, Philipps-Universität Marburg
Hans-Meerwein-Strasse 4, 35032 Marburg (Germany)
E-mail: frenking@chemie.uni-marburg.de

[d] Prof. G. Frenking
Institute of Advanced Synthesis, School of Chemistry and Molecular Engineering, Jiangsu National Synergetic Innovation Center for Advanced Materials, Nanjing Tech University, Nanjing 211816 (China)

[+] These authors contributed equally to this work.

Supporting information and the ORCID identification number(s) for the author(s) of this article can be found under: https://doi.org/10.1002/chem.202002986.

Chemistry–A European Journal

Full Paper
doi.org/10.1002/chem.202002986

Chemistry Europe
European Chemical
Societies Publishing

Ca, Sr and Ba. It seems plausible that the (n)s valence orbital of the atom mixes with the (n)p atomic orbitals (AOs) to give optimal (n)sp^x hybrid orbitals for covalent bonds, which is typical of main-group elements. However, recent studies of molecular complexes of the heavier Ae elements, which were experimentally observed in the gas phase and in low-temperature matrices, suggest that the most important valence orbitals of Ca, Sr and Ba are the $(n-1)$d functions. Analysis of the electronic structures of the octacarbonyls $[Ae(CO)_8]$[8] and the isoelectronic dinitrogen complexes $[Ae(N_2)_8]$[9] as well as the tribenzene adducts $[Ae(Bz)_3]$[10] (Ae = Ca, Sr, Ba) revealed that the covalent part of the metal–ligand bonding comes mainly from Ae→L π backdonation from occupied metal d orbitals into π^* molecular orbitals (MOs) of the ligands, followed by Ae←L σ donation into vacant metal d orbitals. Prior work on the observed redshift of the CO stretching frequency in $Ba(CO)^+$ and $Ba(CO)^-$ provided evidence for strong π backdonation from the occupied $5d(\pi)$ AOs of Ba to the π^* MOs of CO.[11] The relevance of the $(n-1)$d orbitals of the Ae atoms for chemical bonding in the octacarbonyls has been questioned by some authors who suggested that the Ca–$(CO)_8$ bonds may have mainly ionic character[12,13] and that the d orbitals of Ca are irrelevant for Ca→CO π backdonation.[12–14] However, geometry optimisation of $[Ca(CO)_8]$ in which all d AOs of Ca were deleted from the Fock matrix, led to a lengthening of the Ca–$(CO)_8$ bonds by 0.4 Å,[12] which clearly signals the great relevance of the calcium d orbitals for the chemical bonds.

The importance of the d orbitals for the chemical bonds of the heavy alkaline-earth atoms had previously been suggested by other authors, most prominently by Pyykkö, who coined the term "honorary transition metal" for barium.[15] In a theoretical study devoted to the effect of relativity on molecular structure published in 1979, Pyykkö carried out calculations on several small molecules involving alkaline-earth atoms, such as AeX_2 (Ae = Be, Mg, Ca, Sr, Ba; X = H, F, Cl, Br, I) and concluded "We have presented explicit evidence for a considerable d character in the bonding of the heavier group IIa elements. This d character increases from Ca to Sr and, markedly, in Ba."[16] The relevance of the d orbitals of the heavy Ae elements was also pointed out in review articles by Kaupp.[17] Furthermore, Janczyk et al. reported the involvement of $d(\pi)$ orbitals in the polar π bonds of the imides AeNH when Ae = Ca, Sr, Ba, but $p(\pi)$ AOs in MgNH.[18] More recently, Yu and Truhlar performed calculations on CaO using various DFT methods and found that the bond is best described as a polar bond between Ca^+ and O^- in which the single electron in Ca^+ rests in a 3d orbital.[19] Thus, there is strong and yet not undisputed evidence for the importance of d orbitals for the chemical bonds of the heavy Ae atoms Ca, Sr and Ba. Therefore, we decided to analyse the nature of some archetypical bonds in small molecules containing these atoms.

We present herein the results of quantum chemical calculations on the Ae molecules AeO, AeNH and AeH_2 (Ae = Be, Mg, Ca, Sr, Ba). These molecules were chosen because they form single and double bonds with other main-group atoms with different electronegativities. The nature of the bonding was analysed by the natural bond orbital (NBO)[20] and energy decom-

position analysis combined with natural orbitals for chemical valence (EDA-NOCV)[21] approaches, which are charge and energy decomposition methods based on the wave function using MO theory rather than partitioning of the electron density (so-called real-space methods). The covalent bond is due to the interference of the wave function, and the charge density finally formed is the result of such interference.[22] The covalent bond can only be explained at the level of the wave function, and therefore we prefer wave-function-based methods. It is sometimes stated that the EDA-NOCV partitioning scheme has the disadvantage that the results depend on the choice of fragments for the bonding analysis. However, the ability to select different reference states in the EDA-NOCV method allows the determination of the most appropriate fragments for the interpretation of the bond; this is actually a strength and not a weakness of the approach. For example, transition-metal compounds with alkene and alkyne ligands can be distinguished as π-bonded complexes or as metallacyclic species.[23,24] Also, transition-metal compounds with carbene and carbyne ligands may be classified as Fischer or Schrock complexes depending on the electronic state of the metal.[23a,24,25] Real-space partitioning does not provide information on the electronic state of the fragments. Moreover, choosing different fragments may provide answers to different questions on bonding. For example, LiF can be discussed by using neutral atoms Li and F or ions Li^+ and F^- as interacting species. The results obtained by using neutral fragments include all the interactions of the atoms during bond formation. The choice of ionic fragments Li^+ and F^- provides information on the interactions in the finally formed molecule. The EDA-NOCV method thus has a greater flexibility than real-space methods, which give valuable information on the electronic structure but only after bond formation.

Theoretical Methods

The geometrical optimisations followed by harmonic vibrational frequency computations of the molecules were performed at the BP86[26]/def2-TZVPP[27] level of theory. The BP86 functional was chosen for this project because it gave the best agreement for the geometries of the calculated molecules with experimental values and previous high-level calculations, and it proved to be very accurate in another project in which we calculated the geometries of heavy alkaline-earth compounds.[28] This basis set uses quasi-relativistic effective core potentials for 28 and 46 core electrons for Sr and Ba, respectively, and all-electron basis sets for the other atoms. Computations on AeO, AeNH and AeH_2 were carried out by using the Gaussian 16 program package.[29] A superfine integration grid was used for the computations. For the initial geometry optimisations of $Ca_6H_9^{3+}$ and $Ca_6H_9[N(SiMe_3)_2]_3(pmdta)_3$ (pmdta = N,N,N',N'',N''-pentamethyldiethylenetriamine), TurboMole 7.1 optimiser[30] was used and the resolution-of-identity method applied.[31] This level is denoted RI-BP86/def2-TZVPP. For $Ca_6H_9[N(SiMe_3)_2]_3(pmdta)_3$, the reported crystal structure[32] was used as the starting point for the calculations. The optimised structure of $Ca_6H_9^{3+}$ was characterised as a minimum by calculating the Hessian matrix analytically. The NBO calculations were carried out with version 6.0.[33]

Chemistry–A European Journal

Full Paper
doi.org/10.1002/chem.202002986

Chemistry
Europe
European Chemical
Societies Publishing

The bonding situation was further studied by energy decomposition analysis (EDA)[34] combined with the natural orbitals for chemical valence (NOCV)[35] method by using the ADF 2017.01 program package.[36] The EDA-NOCV[21] calculations were performed at the BP86/TZ2P[37] level of theory using the BP86/def2-TZVPP optimised geometries with the scalar relativistic effects included by adopting the zeroth-order regular approximation (ZORA).[38] In the EDA method, the intrinsic interaction energy (ΔE_{int}) between two fragments is decomposed into three energy components [Eq. (1)].

$$\Delta E_{int} = \Delta E_{elstat} + \Delta E_{Pauli} + \Delta E_{orb} \qquad (1)$$

The ΔE_{elstat} term represents the quasi-classical electrostatic interaction between the unperturbed charge distributions of the prepared fragments. The Pauli repulsion ΔE_{Pauli} is the energy change associated with the transformation from the superposition of the unperturbed electron densities of the isolated fragments to the wave function, which properly obeys the Pauli principle through explicit anti-symmetrisation and renormalisation of the product wave function. The term ΔE_{orb} originates from the mixing of orbitals, charge transfer and polarisation between the isolated fragments.

The combination of EDA with the NOCV method allows us to partition the total ΔE_{orb} term into pairwise contributions of the orbital interactions. The electron density deformation $\Delta \rho_k(r)$, which originates from the mixing of the orbital pairs $\Psi_k(r)$ and $\Psi_{-k}(r)$ where k gives the number of occupied orbitals. of the interacting fragments in the complex, represents the amount and the shape of the charge flow due to orbital interactions [Eq. (2)], whereas the associated orbital energy term reflects the strength of such orbital interactions [Eq. (3)].

$$\Delta \rho_{orb}(r) = \sum_k \Delta \rho_k(r) = \sum_{k=1}^{\frac{N}{2}} \nu_k \left[-\Psi_{-k}^2(r) + \Psi_k^2(r) \right] \qquad (2)$$

$$\Delta E_{orb}(r) = \sum_k \Delta E_{orb}^k = \sum_k \nu_k \left[-F_{-k,-k}^{TS} + F_{k,k}^{TS} \right] \qquad (3)$$

Therefore, both qualitative ($\Delta \rho_{orb}$) and quantitative (ΔE_{orb}) information on the strength of individual pairs of orbital interactions can be obtained from an EDA-NOCV analysis. For further details on the EDA-NOCV method and its application to the analysis of the chemical bond, some recent reviews are recommended.[39]

Results

AeO

Table 1 presents the calculated and experimental bond lengths $r(Ae–O)$ and bond dissociation energies (BDEs) D_0 of the alkaline-earth oxides AeO as well as the results of the NBO analysis. The theoretical values for $r(Ae–O)$ and D_0 are in reasonable agreement with the available experimental data. The Wiberg bond order (WBO) is slightly less than 1 for BeO and slightly more than 1 for the heavier homologues of AeO. This could be interpreted as an indication of a covalent single bond, however, the Ae–O bonds are very polar. The atomic partial charges suggest, as expected, large positive charges, more than +1, for the Ae atoms, with the largest value for Be. The WBO values therefore signal multiple bond character. This is in agreement with the NBO analysis, which indicates two bond

Table 1. Calculated bond lengths $r(Ae–O)$, bond dissociation energies D_0, WBOs, partial charges q, polarisation and hybridisation of the NBO bond orbitals of the alkaline-earth oxides AeO.[a]

AeO	$r(Ae–O)$ [Å]	D_0 [kcal mol^{-1}]	WBO	$q(Ae)$ [e]	Polarisation (Ae [%]/O [%])	Ae hybridisation
BeO	1.346 (1.331)[b]	117.3 (106.0)[b]	0.86	1.53	π[c]: 7.1/92.9 σ: 8.9/91.1	π[c]: p$^{1.0}$ σ: s$^{1.0}$p$^{0.1}$
MgO	1.751 (1.749)[b]	66.4 (81.3)[b]	1.10	1.26	σ: 30.1/69.9	σ: s$^{1.0}$p$^{0.1}$
CaO	1.826 (1.822)[b]	117.2 (109.7)[b]	1.09	1.38	π[c]: 6.5/93.5 σ: 18.1/81.9	π[c]: p$^{1.0}$d$^{17.2}$ σ: s$^{1.0}$p$^{1.1}$d$^{3.2}$
SrO	1.931 (1.920)[b]	112.7 (112.5)[b]	1.04	1.41	π[c]: 6.0/94.0 σ: 17.3/82.7	π[c]: p$^{1.0}$d$^{46.2}$ σ: s$^{1.0}$p$^{1.8}$d$^{3.4}$
BaO	2.009 (1.940)[b]	135.2 (133.4)[b]	1.02	1.43	π[c]: 6.2/93.8 σ: 16.0/84.0	π[c]: p$^{1.0}$d$^{92.7}$ σ: s$^{1.0}$p$^{19.5}$d$^{46.6}$

[a] Experimental values are given in parentheses. All values were calculated at the BP86/def2-TZVPP level of theory. [b] See ref. [4]. [c] Degenerate.

orbitals for the alkaline-earth oxides AeO, one σ orbital and one degenerate π orbital, which are strongly polarised towards the oxygen except in the case of MgO. The standard cut-off values of the NBO algorithm yield only a σ bond for magnesium oxide.

It is helpful to discuss at this point the physical nature of the bonds in the alkaline-earth oxide molecules AeO. As mentioned above, polar bonds A–B form due to the interference between atoms A and B with different electronegativities. There is additional electrostatic attraction in the covalent bonds stemming from the overlap of electronic charge distribution of one atom with the nuclear charge of the other.[6, 40] The percentage contribution of the electrostatic attraction is larger in polar bonds than in non-polar bonds, but this must not be confused with ionic bonding, which is a Coulombic attraction in ionic salt compounds and can be approximated by point charges in a crystal. There is no stable molecule with ionic bonds, because the ionisation energy of an atom is always significantly higher than the electron affinity of any other atom of the periodic system. Therefore, we discuss the polar bonds in this paper in terms of a mixture of covalent bonds and electrostatic (Coulombic) attraction. The difference between electrostatic bonding in a polar bond and in an ionic salt is that the former is due to overlapping electronic and nuclear charge, whereas the latter arises from the attraction between opposite charges, which are separated with negligible overlap.

Table 1 also presents the polarisation and hybridisation of the NBO bond orbitals of AeO. The π orbitals and to a lesser extent also the σ orbitals are strongly polarised towards oxygen. The charge distribution suggests that the molecules are best described in terms of the charged fragment Ae$^+$–O$^-$. Because the π backdonation takes place through degenerate π orbitals, the Lewis structure Ae$^+$≡O$^-$ conforms to the bonding situation, except in the case of MgO. The higher polarity of the π orbitals is below the standard criterion for bond orbitals by the NBO method, which gives therefore only a σ bond Mg$^+$–O$^-$. Such a representation does not agree with the conventional understanding of the chemical bond in the alka-

line-earth oxide molecules AeO, but it does illustrate the nature of the orbital interactions (one electron-sharing σ bond and two dative π interactions). We will see below to what extent the different terms contribute to the bonds.

The most interesting result of the NBO analysis is the hybridisation of the Ae−O bond orbitals at the Ae end. The σ bonds of BeO and MgO have nearly pure (n)s character and the π bond of BeO is constituted by a pure 2p AO. In contrast, the π orbitals of the heavier alkaline-earth oxides at Ae are essentially $(n-1)$d orbitals. Also, the dominant contributions of Ae to the σ orbitals in AeO (Ae = Ca, Sr, Ba) come from the $(n-1)$d orbitals. This is remarkable because the $(n-1)$d AOs of the alkaline-earth atoms are considered by the NBO method as Rydberg orbitals and thus they are treated with lower priority than the (n)s AOs. This can lead to significant problems in the bonding analysis of s-block elements.[41] The results of the NBO analysis shown in Table 1 suggest that the most important valence orbitals for the covalent bonding of the heavier alkaline-earth atoms Ca, Sr and Ba are the $(n-1)$d AOs. The shapes of the NBO σ- and π-bonding orbitals are shown in Figure 1. The dominant contributions of the $(n-1)$d AOs of Ca, Sr and Ba are clearly visible. The NBO algorithm also suggests that the (n)p AOs of Ca, Sr and Ba significantly contribute to the σ bonds of the metal oxides (Table 1). This is in conflict with the measured excitation energies (n)s→(n)p of the atoms and the results of the EDA-NOCV analysis, which are presented and discussed further below.

A more detailed and unbiased analysis of the interatomic interactions is achieved through EDA-NOCV calculations. Table 2 shows the results obtained by using differently charged atomic fragments as interacting moieties. The neutral and doubly charged fragments have a singlet electronic state, whereas the singly charged fragments were calculated in their doublet state. It becomes clear that the choice of neutral atoms gives much higher values of the orbital interaction ΔE_{orb} than the use of charged fragments.[42] This indicates that the final bonding situation of AeO is better described in terms of ionic fragments than by neutral species, because the former fragments undergo much weaker deformation during bond formation. Numerous previous studies using a variety of chemical bonds have shown that the size of ΔE_{orb} is a very useful criterion for finding the most suitable fragments.[43] Comparison of the ΔE_{orb} values calculated by using singly and doubly charged fragments suggests that the best description of the chemical bonds in AeO is provided by Ae$^+$–O$^-$. This is in agreement with the atomic partial charges obtained by the NBO method and the recent theoretical work on CaO by Yu and Truhlar.[19]

Table 2 also provides a breakdown of the total orbital interactions ΔE_{orb} into the most important pairwise contributions. There are three dominant interactions, $\Delta E_{orb(1)}$, $\Delta E_{orb(2)}$ and $\Delta E_{orb(3)}$, which contribute more than 90% to ΔE_{orb}. The associated deformation densities $\Delta\rho_1$–$\Delta\rho_3$ and the related atomic fragment orbitals are shown in Figure 2. It becomes clear that $\Delta E_{orb(1)}$ comes from the Ae$^+$–O$^-$ electron-sharing σ bond, whereas $\Delta E_{orb(2)}$ and $\Delta E_{orb(3)}$ come from the degenerate Ae$^+$ ←O$^-$ π backdonation. Note that the energy contribution of the π backdonation is close to 40% of ΔE_{orb}, whereas the elec-

tron-sharing σ bonding provides slightly more than half of the covalent interactions. The EDA-NOCV results thus suggest that the energy contribution of the degenerate π bond in the alkaline-earth oxides is significantly high and that the covalent contribution to the bonding interactions in MgO and the π

Table 2. Results of the EDA-NOCV calculations at the BP86/TZ2P//BP86/def2-TZVPP level of theory for the alkaline-earth oxides AeO using three different fragments. The energy values are given in kcal mol^{-1}

Fragments	Ae(S) + O(S)	Ae$^+$(D) + O$^-$(D)[a]	Ae^{2+}(S) + O^{2-}(S)
BeO			
ΔE_{int}	−185.6	−298.2	−932.7
ΔE_{Pauli}	188.2	134.4	148.5
ΔE_{elstat}[b]	−25.6 (6.9%)	−263.2 (60.8%)	−893.1 (82.6%)
ΔE_{orb}[b]	−348.2 (93.1%)	−169.4 (39.2%)	−188.1 (17.4%)
$\Delta E_{orb(1)}$[c]	−316.5 (90.9%)	−96.1 (56.7%)	−56.3 (29.9%)
$\Delta E_{orb(2)}$[c]	−13.6 (3.9%)	−32.1 (18.9%)	−61.3 (32.6%)
$\Delta E_{orb(3)}$[c]	−13.6 (3.9%)	−32.1 (18.9%)	−61.3 (32.6%)
$\Delta E_{orb(rest)}$[c]	−4.5 (1.3%)	−9.1 (9.5%)	−9.2 (4.9%)
MgO			
ΔE_{int}	−132.5	−212.6	−774.5
ΔE_{Pauli}	99.6	78.2	120.2
ΔE_{elstat}[b]	−22.9 (9.9%)	−219.3 (75.4%)	−762.8 (85.3%)
ΔE_{orb}[b]	−209.2 (90.1%)	−71.6 (24.6%)	−131.9 (14.7%)
$\Delta E_{orb(1)}$[c]	−204.8 (97.9%)	−42.4 (59.2%)	−71.7 (54.5%)
$\Delta E_{orb(2)}$[c]	–	−13.3 (18.6%)	−27.5 (20.8%)
$\Delta E_{orb(3)}$[c]	–	−13.3 (18.6%)	−27.5 (20.8%)
$\Delta E_{orb(rest)}$[c]	−4.4 (2.1%)	−2.6 (3.6%)	−5.2 (3.9%)
CaO			
ΔE_{int}	−186.4	−231.7	−719.4
ΔE_{Pauli}	118.8	149.6	260.0
ΔE_{elstat}[b]	−19.6 (6.4%)	−246.5 (64.6%)	−792.3 (80.9%)
ΔE_{orb}[b]	−285.6 (93.6%)	−134.8 (35.4%)	−187.1 (19.1%)
$\Delta E_{orb(1)}$[c]	−263.9 (92.4%)	−73.3 (54.4%)	−87.7 (46.9%)
$\Delta E_{orb(2)}$[c]	−10.5 (3.7%)	−28.1 (20.8%)	−45.3 (24.2%)
$\Delta E_{orb(3)}$[c]	−10.5 (3.7%)	−28.1 (20.8%)	−45.3 (24.2%)
$\Delta E_{orb(rest)}$[c]	−0.7 (0.2%)	−5.3 (4.0%)	−8.8 (4.7%)
SrO			
ΔE_{int}	−179.7	−215.9	−684.3
ΔE_{Pauli}	115.6	157.8	283.5
ΔE_{elstat}[b]	−20.7 (7.0%)	−246.8 (66.0%)	−781.6 (80.8%)
ΔE_{orb}[b]	−274.6 (93.0%)	−126.9 (34.0%)	−186.2 (19.2%)
$\Delta E_{orb(1)}$[c]	−255.0 (92.9%)	−67.3 (53.0%)	−91.1 (48.9%)
$\Delta E_{orb(2)}$[b]	−8.6 (3.1%)	−26.3 (20.7%)	−42.4 (22.8%)
$\Delta E_{orb(3)}$[c]	−8.6 (3.1%)	−26.3 (20.7%)	−42.4 (22.8%)
$\Delta E_{orb(rest)}$[c]	−2.4 (0.9%)	−7.0 (5.5%)	−10.3 (5.5%)
BaO			
ΔE_{int}	−208.8	−233.7	−678.3
ΔE_{Pauli}	128.0	192.7	350.5
ΔE_{elstat}[b]	−23.5 (7.0%)	−263.3 (61.8%)	−804.0 (78.2%)
ΔE_{orb}[b]	−313.3 (93.0%)	−162.7 (38.2%)	−224.8 (21.8%)
$\Delta E_{orb(1)}$[c]	−284.9 (92.4%)	−88.1 (54.1%)	−112.2 (49.9%)
$\Delta E_{orb(2)}$[c]	−10.7 (3.7%)	−31.5 (19.4%)	−49.2 (21.9%)
$\Delta E_{orb(3)}$[c]	−10.7 (3.7%)	−31.5 (19.4%)	−49.2 (21.9%)
$\Delta E_{orb(rest)}$[c]	−7.0 (0.2%)	−11.6 (7.1%)	−14.2 (6.3%)

[a] The fragments Ae$^+$ and O$^-$ have an electronic doublet state in which the unpaired electron of Ae$^+$ is in the (n)s orbital (^{2}S) and the unpaired electron of O$^-$ is in the p(σ) orbital (^{2}P). [b] The values in parentheses represent the percentage contribution to the total attractive interactions $\Delta E_{elstat} + \Delta E_{orb}$. [c] The values in parentheses represent the percentage contribution to the total orbital interactions ΔE_{orb}.

Chemistry–A European Journal

Full Paper
doi.org/10.1002/chem.202002986

Chemistry
Europe
European Chemical
Societies Publishing

Figure 1. Plots of the NBO σ- and π-bonding orbitals of AeO.

bonding are the lowest among all the AeO species. This agrees with the NBO results, which suggest only a σ bond and no π bonding in MgO. The reader must be aware, however, that the threshold value in the NBO approach to polarisation, which separates a two-centre bonding orbital from an orbital with a single pair, is chosen arbitrarily. The orbital interactions in MgO

show only small differences from those of the other homologues.

Inspection of the shapes of the deformation densities and the associated atomic orbitals of the fragments reveals a significant difference between BeO and MgO on the one hand and the heavier homologues CaO, SrO and BaO on the other. The

Chemistry–A European Journal

Full Paper
doi.org/10.1002/chem.202002986

Chemistry
Europe
European Chemical
Societies Publishing
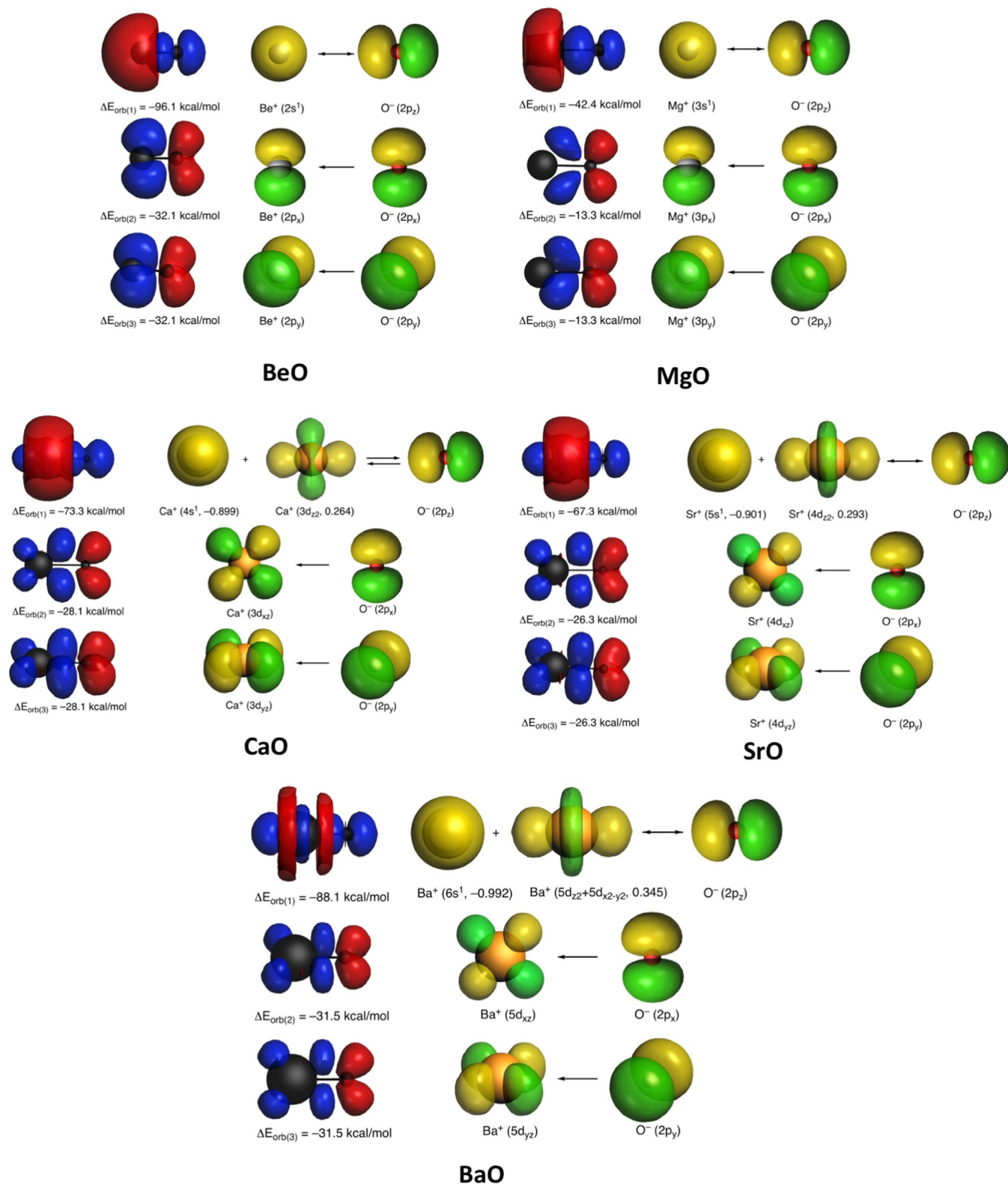
Figure 2. Deformation densities $\Delta\rho_1$–$\Delta\rho_3$ and the associated atomic orbitals of the most important orbital interactions $\Delta E_{\mathrm{orb}(1)}$, $\Delta E_{\mathrm{orb}(2)}$ and $\Delta E_{\mathrm{orb}(3)}$ of AeO using the fragments Ae^+ and O^- (Table 2). The numbers in parentheses of the metal AOs, when more than one AO of a fragment is involved, represent orbital coefficients. The colour code used to represent the flow of charge is red→blue.

$Ae^+\leftarrow O^-$ π backdonation in the heavier systems involves the $d(\pi)$ AOs of the alkaline-earth atoms, whereas π backdonation in BeO and MgO occurs into the $p(\pi)$ orbitals of the metal atoms (Figure 2). Furthermore, the AO composition of the Ae atoms in the Ae^+–O^- electron-sharing σ bond shows large differences between the lighter and heavier atoms. The singly oc-

Chemistry–A European Journal

Full Paper
doi.org/10.1002/chem.202002986

Chemistry
Europe
European Chemical
Societies Publishing

cupied atomic orbitals of Ca, Sr and Ba are hybrids of the (n)s and $(n-1)$d AOs, whereas Be and Mg use only their (n)s orbitals for the electron-sharing σ bond. Thus, the covalent bonding in AeO for Ae = Ca, Sr, Ba involves s/d-hybridised valence orbitals for the σ bonds and d(π) AOs for the π bonds, which is a characteristic feature of transition metals. The EDA-NOCV calculations suggest that the (n)s AO makes a larger contribution than the $(n-1)$d AOs to the σ bonds Ae–O for Ae = Ca, Sr, Ba, whereas the hybridisation of the NBO orbitals indicates that the $(n-1)$d AOs are much more important than the (n)s AO (Table 1). The EDA-NOCV calculations provide information on the energetic consequences of the hybridisation, which appear to be different from the spatial information that comes from the NBO algorithm.

AeNH

Table 3 presents the calculated bond lengths r(Ae–NH) and bond angles along with the BDE values D_0 of the Ae–NH bonds of the alkaline-earth imides AeNH and the results of the NBO analysis. The only experimental result available is for BaNH, which was observed and spectroscopically investigated by rotational spectroscopy by Janczyk et al.[18] These authors also reported the quantum chemical calculations of the homologues AeNH (Ae = Mg, Ca, Sr, Ba). Our calculations predict that the lightest and heaviest homologues, BeNH and BaNH, have a linear geometry, whereas the other imides, MgNH, CaNH and SrNH, possess a bent structure. Our geometries are in good agreement with the values previously reported by Janczyk et al.

The bond dissociation energies calculated for Ae–NH are significantly smaller than those for Ae–O (see Table 1), with D_0 values between 30.5 kcal mol^{-1} (Ae = Mg) and 83.2 kcal mol^{-1} (Ae = Ba), but both series show the same trend. The magnesium compound always has the weakest bond and barium the strongest bond, with the latter twice as strong as the Mg system. In contrast, the WBO values and the strongly positive partial charges of the Ae atoms are quite similar for both the oxides and imides. Interestingly, the Ae atoms in the imides carry a larger positive charge than in the oxides, except in the case of the magnesium compounds, even though nitrogen is less electronegative than oxygen. The NBO method gives three

Ba–NH bond orbitals for linear BaNH, one σ orbital and one degenerate π orbital, which are strongly polarised towards nitrogen. For the linear BeNH, however, only a degenerate π orbital was calculated. The σ orbital has a higher polarity and is classified as a nitrogen lone-pair MO. According to the NBO approach, the Ae–NH bonds of the bent species CaNH and SrNH exhibit one σ-bonding and one π-bonding orbital as well as one lone-pair MO at nitrogen. In contrast, the more strongly bent MgNH has only one Mg–NH σ-bonding orbital and two nitrogen lone-pair MOs. Note that the Mg–NH σ orbital has a much lower polarity than the σ and π orbitals of all the other imides.

The NBO results suggest that the Ae–NH bonds of the imides AeNH possess up to three polarised σ and π orbitals, and the highly polarised orbitals are classified as bonding orbitals or lone-pair MOs, depending on the cut-off criterion of the method. This is not a weakness of the NBO method, but the result of an attempt to describe the bonding situation in terms of Lewis structures. The NBO results can be further elaborated and complemented by the EDA-NOCV calculations, which provide a more detailed insight into the nature of the electronic interactions. We used singly and doubly charged fragments as interacting moieties for the analysis of the Ae–NH bonds. The use of singly charged fragments Ae$^+$ and NH$^-$ in the calculations of the bent structures of MgNH, CaNH and SrNH gave significantly smaller ΔE_{orb} values than the doubly charged Ae^{2+} and NH^{2-}. Slightly smaller ΔE_{orb} values were also calculated when singly charged fragments were used for the linear BeNH, whereas the opposite was found for BaNH. For the latter species we obtained slightly smaller ΔE_{orb} values when the doubly charged moieties Ba^{2+} and NH^{2-} were used. Because the difference between the ΔE_{orb} values determined for singly and doubly charged fragments of BaNH was not very large, we present the EDA-NOCV results obtained with the singly charged fragments, which allows comparison of all the imides AeNH with the same type of interacting fragments. The results are shown in Table 4. The EDA-NOCV results obtained by using doubly charged fragments are given in Table S1 in the Supporting Information.

The data in Table 4 suggest that the covalent (orbital) contribution to the Ae–NH attraction is between 51% (Ae = Be) and 23% (Ae = Mg). The orbital interactions in the linear species

Table 3. Calculated bond lengths r(Ae–NH), bond angles ∡ (Ae-N-H), bond dissociation energies D_0, WBO values, partial charges q, polarisation and hybridisation of the NBO bond orbitals for the alkaline-earth imides AeNH.[a]

AeNH	r(Ae–NH) [Å]	∡(Ae-N-H) [°]	D_0 [kcal mol^{-1}]	WBO	q(Ae) [e]	Polarisation (Ae [%]/NH [%])	Ae hybridisation
BeNH	1.432	180.0	67.9	0.80	1.56	π[b]: 8.9/91.1	π[b]: p$^{1.0}$
MgNH	1.870	108.9	30.5	1.17	1.06	σ: 41.7/58.3	σ: s$^{1.0}$
CaNH	1.898	167.9	66.5	0.96	1.46	π: 8.6/91.4	π: p$^{1.0}$d$^{8.1}$
						σ: 12.4/87.6	σ: s$^{1.0}$p$^{0.5}$d$^{2.8}$
SrNH	2.013	170.4	62.2	0.94	1.48	π: 8.3/91.7	π: p$^{1.0}$d$^{15.7}$
						σ: 11.0/89.0	σ: s$^{1.0}$p$^{0.5}$d$^{4.0}$
BaNH	2.117 (2.08)[c]	180.0 (180)[c]	83.2	0.91	1.49	π[b]: 8.8/91.2	π[b]: p$^{1.0}$d$^{40.0}$
						σ: 7.4/92.6	σ: s$^{1.0}$p$^{1.2}$d$^{8.1}$

[a] Experimental values are given in parentheses. All values were calculated at the BP86/def2-TZVPP level of theory. [b] Degenerate. [c] Ref. [18].

Chemistry–A European Journal

Full Paper
doi.org/10.1002/chem.202002986

Chemistry Europe
European Chemical
Societies Publishing

Table 4. Results of the EDA-NOCV calculations at the BP86/TZ2P//BP86/def2-TZVPP level of theory for the alkaline-earth imides AeNH.

Fragments	BeNH	MgNH	CaNH	SrNH	BaNH
$Ae^+(^2S) + NH^{-[a]}$					
ΔE_{int}	−361.1	−206.8	−209.6	−193.5	−291.1
ΔE_{Pauli}	77.7	78.6	188.0	195.6	134.6
$\Delta E_{elstat}^{[b]}$	−216.6	−220.1	−283.1	−281.6	−222.6
	(49.4%)	(77.1%)	(71.2%)	(72.4%)	(52.3%)
$\Delta E_{orb}^{[b]}$	−222.2	−65.4	−114.5	−107.4	−203.1
	(50.6%)	(22.9%)	(28.8%)	(27.6%)	(47.7%)
$\Delta E_{orb(1)}^{[c]}$	−138.9	−35.9	−46.0	−40.1	−127.3
	(62.6%)	(54.9%)	(40.2%)	(37.3%)	(62.7%)
$\Delta E_{orb(2)}^{[c]}$	−40.3	−16.2	−31.6	−29.1	−33.7
	(18.1%)	(24.8%)	(27.6%)	(27.1%)	(16.6%)
$\Delta E_{orb(3)}^{[c]}$	−40.3	−11.2	−33.0	−33.6	−33.7
	(18.1%)	(17.1%)	(28.8%)	(31.3%)	(16.6%)
$\Delta E_{orb(rest)}^{[c]}$	−2.7	−2.1	−3.9	−4.6	−8.4
	(1.2%)	(3.2%)	(3.4%)	(4.3%)	(4.1%)

[a] The fragments Ae^+ and NH^- of all systems except Ae=Mg have an electronic doublet state in which the unpaired electron of Ae^+ is in the $(n)s$ orbital and the unpaired electron of NH^- is in a σ orbital ($^2\Sigma$). In CaNH and SrNH, the unpaired electron of NH^- in the electronically excited ($^2\Pi$) state is in a π orbital, which is the in-plane $\pi_\parallel$ orbital of the NH fragment, which can mix with an $(n)s/(n−1)d$ hybrid AO of Ca and Sr. The electronic reference state of NH^- for linear BeNH and BaNH and the strongly bent MgNH is the electronically excited ($^2\Sigma^+$) state in which the unpaired electron is in a σ orbital. [b] The values in parentheses represent the percentage contribution to the total attractive interactions $\Delta E_{elstat} + \Delta E_{orb}$. [c] The values in parentheses represent the percentage contribution to the total orbital interactions ΔE_{orb}.

BeNH and BaNH exhibit one dominant pairwise term $\Delta E_{orb(1)}$, which provides 63% of ΔE_{orb}, and the degenerate pair $\Delta E_{orb(2)}$ and $\Delta E_{orb(3)}$, which contribute around one third of the total orbital interactions. Figure 3 shows the deformation densities $\Delta\rho_1–\Delta\rho_3$ and the associated orbitals of the fragments corresponding to $\Delta E_{orb(1)}$, $\Delta E_{orb(2)}$ and $\Delta E_{orb(3)}$. It is evident that $\Delta E_{orb(1)}$ comes from the coupling of the unpaired electrons, which gives the electron-sharing σ bond, whereas $\Delta E_{orb(2)}$ and $\Delta E_{orb(3)}$ come from the degenerate $Ae^+\leftarrow NH^-$ π backdonation. The σ orbital of BeNH is mainly formed by the 2s AO of Be at the metal, whereas Ba uses a hybrid of the 6s and 5d(σ) AOs for the Ba−NH σ orbital. The acceptor orbitals of the $Ae^+ \leftarrow NH^-$ π backdonation are the p(π) AOs of Be and the d(π) AOs of Ba.

The data in Table 4 show that the orbital contributions to the bent structures of MgNH, CaNH and SrNH are significantly lower than those to the linear structures of BeNH and BaNH. There are also three major pairwise contributions $\Delta E_{orb(1)}$, $\Delta E_{orb(2)}$ and $\Delta E_{orb(3)}$ to the bent structures, which can be identified with the help of the associated deformation densities $\Delta\rho$ and the fragment orbitals shown in Figure 3. There is an interesting difference between the strongly bent MgNH and the more weakly bent CaNH and SrNH. The electron-sharing bond of MgNH ($\Delta E_{orb(1)}$) arises from the coupling of the unpaired electron in the σ orbital of NH^- in the electronically excited ($^2\Sigma^+$) state with the electron in the Mg^+ 3s AO. In contrast, the electron-sharing bonds in CaNH and SrNH are due to the coupling of the unpaired electron in the π orbital of NH^- in the ($^2\Pi$) ground state with the electron of Ca^+ or Sr^+ in an $(n)s/$

$(n−1)d$ hybrid AO. The orbital interactions $\Delta E_{orb(2)}$ and $\Delta E_{orb(3)}$ in MgNH stem from $Mg^+\leftarrow NH^-$ π backdonation into the vacant 3p(π) AOs of Mg. The backdonation $Ae^+\leftarrow NH^-$ in CaNH and SrNH occurs through one π and one σ donation into vacant d AOs of Ae^+. Note that the symmetry assignments refer to the diatomic species NH^-. The in-plane $\pi_\parallel$ orbital of the NH^- fragment can mix with the Ae^+ σ orbitals and therefore only two bonds with σ and π symmetry remain for the bent AeNH species, in agreement with the NBO results.

The most important result of this section concerns the nature of the valence orbitals of Ca, Sr and Ba. The NBO and EDA-NOCV results clearly show that the covalent bonding of the heavier alkaline-earth atoms in the imides AeNH is due to the s/d hybrid valence AOs for σ bonds and d AOs for π bonds, which is a characteristic feature of bonding in transition metals.

AeH$_2$

The alkaline-earth dihydrides have been the topic of numerous theoretical and experimental studies before. Although little experimental geometrical data have been reported, combining the data that is available with accurate quantum chemical calculations provides reliable information on the structures of AeH_2. The lightest members, BeH_2 and MgH_2, have a linear geometry, whereas SrH_2 and BaH_2 are definitely bent.[44–53] However, the equilibrium geometry of CaH_2 remained unclear for a long time. Early quantum chemical calculations suggested a linear structure, but experimental studies indicated a bent structure with angles of 168 and 166°.[44,46d] Highly accurate coupled-cluster calculations at the CCSD(T) level of theory using large basis sets found an energy minimum with a bending angle of 164° and a very flat potential with a barrier to linearity of only 6 cm^{-1}.[54] The molecule CaH_2 may therefore be considered as quasi-linear. The data in Table 5 show that the geometries calculated at the BP86/def2-TZVPP level agree well with those suggested by experimental data and the most accurate theoretical values previously reported in the literature. The bending angles of the heavier molecules CaH_2, SrH_2 and BaH_2 are more acute than previous values, but this does not affect the results of the bonding situation.

The calculations suggest that BeH_2 has the strongest bonds with an average D_0 of 72 kcal mol^{-1}, whereas the heavier dihydrides possess rather uniform values of $D_0 = 50 \pm 3$ kcal mol^{-1} for the Ae−H bonds. The Wiberg bond indices and the NBO data indicate strongly polar single bonds $Ae^{\delta+}–H^{\delta-}$. The atomic valence orbitals of Be and Mg that are engaged in the bonds are mainly the $(n)s$ orbitals with a small admixture of $(n)p$ AOs, whereas the valence orbitals of Ca, Sr and Ba are hybrids of $(n)s$ and $(n−1)d$ AOs.

We carried out EDA-NOCV calculations on AeH_2 by using singly and doubly charged fragments as the interacting species. The calculations show that the orbital term is always smaller for the Ae^+ and $(H_2)^-$ fragments than for the doubly charged Ae^{2+} and $(H_2)^{2-}$, except in the case of BaH_2, when the two pairs gave nearly identical values for ΔE_{orb}. Table 6 presents the results of the EDA-NOCV calculations using Ae^+ and

Chemistry–A European Journal

Full Paper
doi.org/10.1002/chem.202002986

Chemistry Europe
European Chemical
Societies Publishing

Figure 3. Deformation densities $\Delta\rho_1$–$\Delta\rho_3$ and the associated atomic orbitals of the most important orbital interactions $\Delta E_{orb(1)}$, $\Delta E_{orb(2)}$ and $\Delta E_{orb(3)}$ of AeNH using the fragments Ae^+ and NH^- (Table 4). The numbers in parentheses of the metal AOs, when more than one AO of a fragment is involved, represent orbital coefficients. The colour code used to represent the flow of charge is red→blue.

$(H_2)^-$ as fragments. The results using the doubly charged fragments Ae^{2+} and $(H_2)^{2-}$ are presented in Table S2 in the Supporting Information. The data in Table 6 indicate that 46% of the interactions in BeH_2 come from covalent bonding between Be^+ and $(H_2)^-$, whereas the attractive interactions between

Ae^+ and $(H_2)^-$ in the heavier homologues possess 30% covalent character. There are two main pairwise components in all the molecules. $\Delta E_{orb(1)}$ comes from the coupling of the unpaired electrons of the fragments, which initially occupy the $(n)s$ AO of Ae^+ and the σ_g MO of the $(H_2)^-$ moiety. The second

Table 5. Calculated bond lengths r(Ae–H), bond angles ∡(H-Ae-H), bond dissociation energies D_0 (A + 2H), WBOs, partial charges q, polarisation and hybridisation of the NBO bond orbitals for the alkaline-earth dihydrides AeH$_2$.[a]

AeH$_2$	r(Ae–H) [Å]	∡(H-Ae-H) [°]	D_0 [kcal mol^{-1}]	WBO	q(Ae) [e]	Polarisation (Ae [%]/H [%])	Ae hybridisation
BeH$_2$	1.343 (1.326)[b]	180 (180)[b]	144.8	0.56	1.15	18.2/81.8	s$^{1.0}$p$^{0.1}$
MgH$_2$	1.714 (1.718)[c]	180 (180)[c]	101.0	0.48	1.29	13.6/86.4	s$^{1.0}$p$^{0.1}$
CaH$_2$	2.018 (2.048)[d]	135.0 (164.0)[d]	105.1	0.43	1.47	11.7/88.3	s$^{1.0}$d$^{0.4}$
SrH$_2$	2.153 (2.201)[e]	120.5 (139.6)[e]	97.8	0.46	1.43	13.2/86.8	s$^{1.0}$d$^{0.4}$
BaH$_2$	2.277 (2.314)[e]	110.5 (118.7)[e]	106.1	0.48	1.44	13.8/86.2	s$^{1.0}$d$^{0.9}$

[a] Experimental or previously reported most accurate ab initio values are given in parentheses. All values were calculated at the BP86/def2-TZVPP level of theory. [b] Experimental value, see ref. [46b]. [c] Calculated value, see ref. [44b]. [d] Calculated value, see ref. [54]. [e] Calculated value, see ref. [48b].

Table 6. Results of the EDA-NOCV calculations at the BP86/TZ2P//BP86/def2-TZVPP level of theory for the alkaline-earth dihydrides AeH$_2$.

Fragments	BeH$_2$	MgH$_2$	CaH$_2$	SrH$_2$	BaH$_2$
Ae$^+$ (^{2}S) + (H$_2$)$^-$ ($^2\Sigma_g$)					
ΔE_{int}	−351.0	−258.1	−223.6	−207.5	−205.7
ΔE_{Pauli}	8.3	28.9	55.8	66.2	82.8
ΔE_{elstat}[a]	−194.5 (54.1%)	−199.9 (69.3%)	−195.8 (70.0%)	−194.1 (70.9%)	−196.8 (68.2%)
ΔE_{orb}[a]	−164.7 (45.9%)	−87.2 (30.4%)	−83.7 (30.0%)	−79.7 (29.1%)	−91.7 (31.8%)
$\Delta E_{orb(1)}$[b]	−70.6 (42.9%)	−58.7 (67.3%)	−60.9 (72.8%)	−53.9 (67.6%)	−55.8 (60.9%)
$\Delta E_{orb(2)}$[b]	−94.1 (57.1%)	−23.4 (26.8%)	−21.9 (26.2%)	−24.2 (30.4%)	−33.2 (36.2%)
$\Delta E_{orb(rest)}$[b]	−0.0 (0.0%)	−5.1 (5.8%)	−0.9 (1.0%)	−1.6 (2.0%)	−2.7 (1.9%)

[a] The values in parentheses represent the percentage contribution to the total attractive interactions $\Delta E_{elstat} + \Delta E_{orb}$. [b] The values in parentheses represent the percentage contribution to the total orbital interactions ΔE_{orb}.

major contribution $\Delta E_{orb(2)}$ is due to the donation Ae$^+$←(H$_2$)$^-$ from the doubly occupied σ_u MO of (H$_2$)$^-$ to the vacant AOs of Ae$^+$. We would like to point out that the electron-sharing interaction $\Delta E_{orb(1)}$ is as usual stronger than the dative bonding $\Delta E_{orb(2)}$, except in the case of BeH$_2$. In the latter case, we find the reverse situation with the dative interaction being stronger than the electron-sharing bond, which is surprising. This might be due to the more effective overlap of the orbitals involved in the dative interactions.

The associated deformation densities $\Delta\rho$ and fragment orbitals shown in Figure 4 display the flow of charge and the nature of the atomic orbitals involved in the covalent terms $\Delta E_{orb(1)}$ and $\Delta E_{orb(2)}$. It becomes clear that the electron-sharing interactions $\Delta E_{orb(1)}$ of BeH$_2$ and MgH$_2$ use only the (n)s AO of the metal atom, whereas the metal orbitals of the heavier systems Ca, Sr and Ba are hybrids of (n)s and $(n-1)$d$_{z^2}$ orbitals. The metal acceptor orbitals of the dative interaction Ae$^+$←(H$_2$)$^-$ are (n)p$_\sigma$ AOs when Ae = Be, Mg, whereas the heaviest metals Sr and Ba use their $(n-1)$d$_{xz}$ AOs as acceptor orbitals.

The acceptor orbital of Ca in CaH$_2$, which has a wider bond angle than SrH$_2$ and BaH$_2$, is a hybrid of the (n)p$_\sigma$ AO and $(n-1)$d$_{xz}$ AO. These results further confirm that the heavier alkaline-earth atoms in the dihydrides AeH$_2$, similarly to the oxides AeO and imides AeNH, use s/d hybrid valence AOs for σ bonds and d AOs for π bonds, which is a characteristic of the chemical bonds of transition metals. We would like to point out that this result does not depend on the choice of the interacting fragments. The s/d hybrid valence AOs of Ca, Sr and Ba are also the acceptor orbitals when doubly charged fragments Ae^{2+} and (H$_2$)$^{2-}$ are used (see Figure S1 in the Supporting Information).

Ca$_6$H$_9$[N(SiMe$_3$)$_2$]$_3$(pmdta)$_3$

The alkaline-earth oxides AeO, imides AeNH and dihydrides AeH$_2$ discussed above are examples of isolated molecules that exist in the gas phase or in inert matrices but agglomerate in a condensed phase where the binding situation becomes significantly different. Molecular compounds of the alkaline-earth metals play an important role in many reactions and their relevance has lately been demonstrated by several surprising findings in the field of catalytic activity in imine and alkene hydrogenation and organocalcium-mediated nucleophilic alkylation of benzene.[55–58] As an example, we cite the recent study of Harder and co-workers, who reported simple alkaline-earth catalysts for effective alkene hydrogenation.[55a] The central species of the catalytic reaction is the cluster complex Ca$_6$H$_9$[N(SiMe$_3$)$_2$]$_3$(pmdta)$_3$ (**A**, Figure 5a), which was previously isolated and structurally characterised by X-ray crystallography.[32] The complex consists of a Ca$_6$H$_9^{3+}$ trication as the core unit with an endohedral hydrogen atom in the centre of a Ca$_6$H$_8^q$ cage (Figure 5b). Three of the calcium atoms carry pmdta ligands, and the other three are each bound to a N(SiMe$_3$)$_2^-$ substituent, which yields the neutral complex **A**.

We analysed the bonding situation of the calcium atoms in **A** and in the central Ca$_6$H$_9^{3+}$ core unit by considering a single Ca^q ($q = 0, +1, +2$) atom/ion and the remaining fragments as interacting species. The smallest orbital values were obtained when doubly charged Ca^{2+} was taken as the metal ion. This is

Chemistry–A European Journal

Full Paper
doi.org/10.1002/chem.202002986

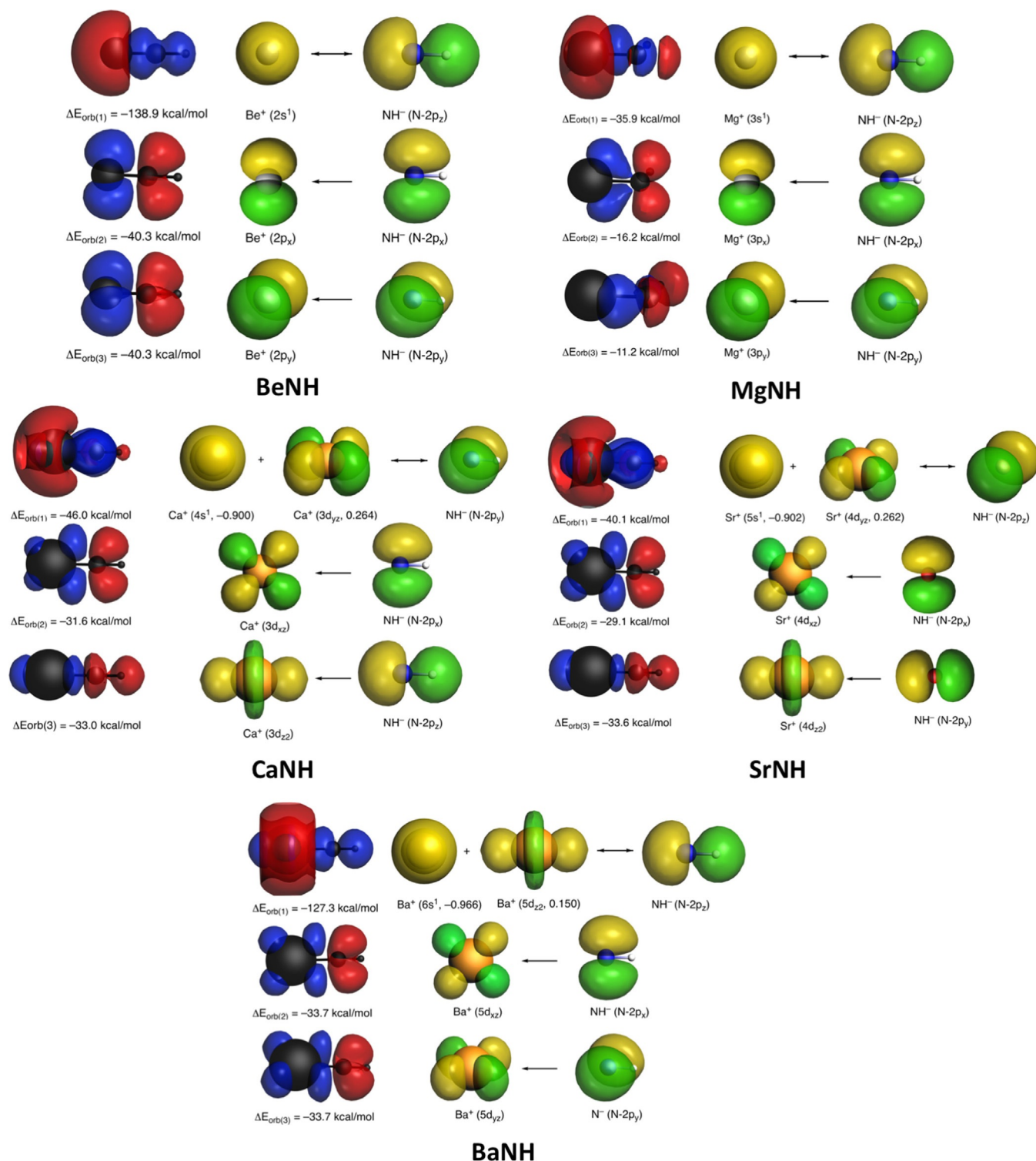**Chemistry Europe**
European Chemical
Societies Publishing

Figure 4. Deformation densities $\Delta\rho_1$ and $\Delta\rho_2$ and the associated atomic orbitals of the most important orbital interactions $\Delta E_{orb(1)}$ and $\Delta E_{orb(2)}$ of AeH$_2$ using the fragments Ae$^+$ and (H$_2$)$^-$ (Table 6). The numbers in parentheses of the metal AOs, when more than one AO of a fragment is involved, represent orbital co-efficients. The colour code used to represent the flow of charge is red$\rightarrow$blue.

in agreement with the calculated charge distribution of the atoms (Figure 5). The NBO method suggests that the calcium atoms in **A** carry positive charges of between $+1.63e$ and $+1.69e$, whereas the hydrogen atoms of the cage have nega-tive charge of between $-0.81e$ and $-0.82e$ for the peripheral atoms (H^{per}) and $-0.89e$ for the central hydrogen (H^{cen}). The charge distribution in the naked octahedral (O_h) Ca$_6$H$_9^{3+}$ core unit is only slightly different: the equivalent calcium atoms have a positive charge of $+1.70e$ and the peripheral hydrogen atoms carry a negative charge of $-0.79e$ and the central hy-drogen atom has a negative charge of $-0.88e$.

Table 7 presents the results of the EDA-NOCV calculations. The data suggest that the interatomic interactions of the four slightly different calcium atoms in **A** are not very different, and that one third of the bonding forces are covalent and two thirds are due to electrostatic attraction. In contrast, the bind-ing forces of calcium in the unsubstituted core trication

Ca$_6$H$_9^{3+}$ come mainly from orbital interactions, which contrib-ute more than 85 % to the total attraction towards the hydridic hydrogen atoms. The EDA-NOCV calculations on **A** using Ca$_6$H$_9^{3+}$ and the ligands [{N(SiMe$_3$)$_2$}$_3$(pmdta)$_3$]$^{3-}$ indicate that the bonds between calcium and the ligands stem mainly from Coulombic attraction, which contributes 75 % to the attractive interactions. The EDA-NOCV calculations suggest that the Ca–H bonds in **A** are mainly covalent, whereas the Ca–ligand bonds are mainly electrostatic.

The focus of this section is on the nature of the valence or-bitals of Ca used in the covalent interactions. To this end we inspected the most important pairwise interactions of the orbi-tal term ΔE_{orb} in the bonding between Ca^{2+} and the remaining fragment in compound **A** and in the trication Ca$_6$H$_9^{3+}$. There are five contributions, each greater than 15 kcal mol^{-1}, in the five different fragmentation schemes in which Ca^{2+} is involved as a fragment (Table 7). All the pairwise contributions come

Chemistry–A European Journal

Full Paper
doi.org/10.1002/chem.202002986

Chemistry
Europe
European Chemical
Societies Publishing

(a) $Ca_6H_9(N(SiMe_3)_2)_3(PMDTA)_3$ **A**

(b) $Ca_6H_9^{3+}$

$q(Ca^{(1)}/Ca^{(2)}/Ca^{(3)}) = +1.63/+1.64/+1.64^a$
$q(Ca^{(4)}/Ca^{(5)}/Ca^{(6)}) = +1.68/+1.69/+1.69^b$
$q(H^{per}) = -0.81/-0.82^c$
$q(H^{cen}) = -0.89^d$
$q(Ca_6H_9^{3+}) = +2.57$

$q(Ca) = +1.70$
$q(H^{per}) = -0.79^a$
$q(H^{cen}) = -0.88^b$

aSlightly different values because of the
conformations of the $N(SiMe_3)_2$ ligands
bSlightly different values because of the
conformations of the PMDTA ligands
cSlightly different values of the peripheral
hydrogen atoms due to conformations of the
ligands.
dCentral hydrogen atom

aPeripheral hydrogen atoms
bCentral hydrogen atom

Figure 5. Geometries of a) the alkaline-earth cluster **A** and b) its central species $Ca_6H_9^{3+}$ as well as the atomic partial charges q of Ca and the hydrogen atoms of the central $Ca_6H_9^{3+}$ fragment calculated at the RI-BP86/def2-TZVPP level of theory.

Table 7. Results of the EDA-NOCV calculations at the BP86/TZ2P//RI-BP86/def2-TZVPP level of theory for the alkaline-earth compounds **A** and $(Ca_6H_9)^{3+}$.

Molecules	$Ca_6H_9[N(SiMe_3)_2]_3(pmdta)_3$ **A**					$(Ca_6H_9)^{3+}$
fragments[a]	$Ca^{(1)2+} + (Ca_5H_9)Lig^{2-}$	$Ca^{(2/3)2+} + (Ca_5H_9)Lig^{2-}$	$Ca^{(4/5)2+} + (Ca_5H_9)Lig^{2-}$	$Ca^{(6)2+} + (Ca_5H_9)Lig^{2-}$	$(Ca_6H_9)^{3+} + Lig^{3-}$	$Ca^{2+} + (Ca_5H_9)^+$
ΔE_{int}	−557.5	−565.5	−570.8	−576.8	−788.77	−98.1
ΔE_{Pauli}	95.8	86.1	102.1	101.7	260.7	70.8
ΔE_{elstat}[b]	−433.2 (66.3%)	−434.5 (66.7%)	−451.7 (67.1%)	−458.6 (67.6%)	−799.5 (76.2%)	−20.1 (11.9%)
ΔE_{orb}[b]	−220.1 (33.7%)	−217.2 (33.3%)	−221.3 (32.9%)	−219.9 (32.4%)	−249.8 (23.8%)	−148.9 (88.1%)
$\Delta E_{orb(1)}$[c]	−34.6 (15.7%)	−30.0 (13.8%)	−32.4 (14.6%)	−31.9 (14.5%)	−35.7 (14.3%)	−32.8 (22.0%)
$\Delta E_{orb(2)}$[c]	−29.3 (13.3%)	−25.0 (11.5%)	−29.1 (13.1%)	−28.5 (13.0%)	−35.3 (14.1%)	−28.0 (18.9%)
$\Delta E_{orb(3)}$[c]	−25.7 (11.7%)	−24.8 (11.4%)	−24.4 (11.0%)	−24.6 (11.2%)	−32.7 (13.1%)	−27.2 (18.3%)
$\Delta E_{orb(4)}$[c]	−24.5 (11.1%)	−23.0 (10.6%)	−23.1 (10.4%)	−23.0 (10.5%)	−16.8 (6.7%)	−27.2 (18.3%)
$\Delta E_{orb(5)}$[c]	−19.5 (8.9%)	−19.5 (9.0%)	−21.4 (9.7%)	−21.0 (9.5%)	−16.6 (6.6%)	−19.2 (12.9%)
$\Delta E_{orb(rest)}$[c]	−86.5 (39.3%)	−94.9 (43.7%)	−90.9 (41.1%)	−90.9 (41.3%)	−112.7 (45.1%)	−14.5 (9.7%)

[a] Lig indicates the sum of the substituents $[N(SiMe_3)_2]_3(pmdta)_3$. [b] The values in parentheses represent the percentage contribution to the total attractive interactions $\Delta E_{elstat} + \Delta E_{orb}$. [c] The values in parentheses represent the percentage contribution to the total orbital interactions ΔE_{orb}.

Chemistry–A European Journal

Full Paper
doi.org/10.1002/chem.202002986

Chemistry Europe
European Chemical
Societies Publishing

mainly from the donation of the hydridic hydrogen atoms to the vacant atomic orbitals of Ca^{2+}. The donation of the ligands $[\{N(SiMe_3)_2\}_3(pmdta)_3]^{3-}$ is much smaller. This agrees with the finding that the interactions of the ligands with the $Ca_6H_9^{3+}$ cluster are mainly electrostatic in character.

Figure 6 shows the deformation densities $\Delta\rho_1-\Delta\rho_5$ and the corresponding fragment orbitals associated with the pairwise orbital terms $\Delta E_{orb(1)}-\Delta E_{orb(5)}$ of $Ca_6H_9^{3+}$ (Table 7). The very similar deformation densities and fragment orbitals determined by the EDA-NOCV calculations on the full complex **A** using Ca^{2+} as a fragment are given in Figure S5 in the Supporting Information. The acceptor valence orbitals of Ca^{2+} are four 3d AOs and the 4s AO. One 3d AO, $d_{x^2-y^2}$, is missing because its symmetry prevents significant overlap with the occupied MOs of the $Ca_5H_9^{2+}$ donor orbitals, which have electron density located on the hydrogen atoms while the $d_{x^2-y^2}$ orbital lobes point towards the interstitial space between them. The pairwise orbital interactions in **A** using $(Ca_6H_9)^{3+}$ and Lig^{3-} involve delocalised orbitals, which are irrelevant for the present study.

The EDA-NOCV and NBO calculations suggest that the chemical bonds between the ligands $[\{N(SiMe_3)_2\}_3(pmdta)_3]^{3-}$ and the $Ca_6H_9^{3+}$ cage are mainly electrostatic in nature, whereas the Ca–H bonds in the central $Ca_6H_9^{3+}$ cluster have mainly covalent character. The most important valence orbitals of calcium in the chemical bonds of **A** are the 3d and 4s AOs.

Discussion

The above results for the valence orbitals of the alkaline-earth metals shall be discussed in the light of the experimentally observed excitation energies of the neutral atoms Ae and the atomic ions Ae^+ from their electronic ground states in which only the (n)s valence orbital is occupied in the lowest-lying excited states with one electron occupying a p or d AO. The measured values are presented in Table 8.[59]

The excitation energies for the neutral atoms show that the values for the excitations s→d of the heavier atoms Ca, Sr and Ba are quite different from the values for the lighter atoms Be and Mg. The ^3D $(2s^13d^1)$ state of Be and the ^1D $(3s^13d^1)$ state of Mg are high-lying excited states of the lighter Ae atoms. In contrast, the ^3D $((n)s^1(n-1)d^1)$ states, which are the second ex-

cited states for Ca and Sr and the first excited state of Ba, are much lower in energy. More relevant for the covalent bonds in the molecules presented above are the excited states of the atomic ions Ae^+, for which the heavier atoms Ca, Sr and Ba again exhibit different features from Be and Mg. The most important finding is that the ^2D $((n-1)d^1)$ states of Ca, Sr and Ba are the lowest-lying excited states of the heavier ions, whereas the first excited state of Be and Mg is the ^2P $((n)p^1)$ state. This explains why the π bonds of Ca, Sr and Ba use their d(π) AOs for covalent bonds instead of the p(π) AOs as is usual for main-group atoms.

The low excitation energies of the ^2D $((n-1)d^1)$ states of Ca^+, Sr^+ and Ba^+ must not be taken as an indication that the covalent bonds of the alkaline-earth atoms occur through their electronically excited states. The EDA-NOCV calculations on AeO, AeNH and AeH_2 (Ae = Ca, Sr, Ba) suggest that the molecules possess electron-sharing σ bonds involving Ae^+ with L^- (L = O, NH, H_2), in which the electron of Ae^+ occupies an s/d(σ) hybrid orbital, that is, the electronic reference state of Ae^+ is the ^2S $((n)s^1)$ ground state. The mixing of the (n)s AO with the $(n-1)$d AO leads to optimal hybrid AOs for covalent σ bonds in a similar way to the familiar sp^x hybridisation of typical main-group atoms. The π bonds of Ca, Sr and Ba use their $(n-1)d(π)$ AOs for covalent interactions because they are energetically lower lying than the (n)p AOs.

In the context of this study it is important to understand how the nature of the covalent bond differs from that of the ionic bond. Covalent bonding is caused by the interference of the electronic wave functions Ψ of the atoms, which leads to a reduction of the kinetic energy density and often also to an accumulation of the electronic charge distribution in the interatomic region.[60] The bond formation can only be understood when the electronic charge distribution is described in terms of the wave function Ψ.[22b,c] After the bond has been formed, the new charge distribution can unambiguously be obtained from the new molecular wave function, because there is a unique definition $\Psi\rightarrow\rho$, with no inverse functional attribution in the other direction $\Psi\leftarrow\rho$. Ruedenberg and co-workers have shown that the energetic stabilisation due to covalent bond formation comes from the lowering of the kinetic energy density of the electrons in the bonding region.[60] Further covalent

Table 8. Measured excitation energies of alkaline-earth atoms and cations from the electronic ground states to the lowest-lying excited states in which one electron is in a p or d orbital.[a]

Ae		Excitation		ΔE [kcal mol^{-1}]	Ae^+		Excitation		ΔE [kcal mol^{-1}]
Be	^1S $(2s^2)$	→	^3P $(2s^12p^1)$[b]	62.8	Be^+	^2S $(2s^1)$	→	^2P $(2p^1)$[b]	91.2
		→	^3D $(2s^13d^1)$[c]	177.3			→	^2D $(3d^1)$[d]	280.2
Mg	^1S $(3s^2)$	→	^3P $(3s^13p^1)$[b]	62.4	Mg^+	^2S $(3s^1)$	→	^2P $(3p^1)$[b]	101.9
		→	^1D $(3s^13d^1)$[e]	132.6			→	^2D $(3d^1)$[f]	204.3
Ca	^1S $(4s^2)$	→	^3P $(4s^14p^1)$[b]	43.3	Ca^+	^2S $(4s^1)$	→	^2P $(4p^1)$[g]	72.0
		→	^3D $(4s^13d^1)$[g]	58.1			→	^2D $(3d^1)$[b]	39.0
Sr	^1S $(5s^2)$	→	^3P $(5s^15p^1)$[b]	40.9	Sr^+	^2S $(5s^1)$	→	^2P $(5p^1)$[g]	67.8
		→	^3D $(5s^14d^1)$[g]	51.9			→	^2D $(4d^1)$[b]	41.6
Ba	^1S $(6s^2)$	→	^3P $(6s^16p^1)$[f]	35.0	Ba^+	^2S $(6s^1)$	→	^2P $(6p^1)$[g]	57.9
		→	^3D $(6s^15d^1)$[b]	25.8			→	^2D $(5d^1)$[b]	13.9

[a] The values are taken from ref. [59]. [b] First excited state. [c] Ninth excited state. [d] Fourth excited state. [e] Fifth excited state. [g] Second excited state. [f] Third excited state.

Chemistry–A European Journal

Full Paper
doi.org/10.1002/chem.202002986

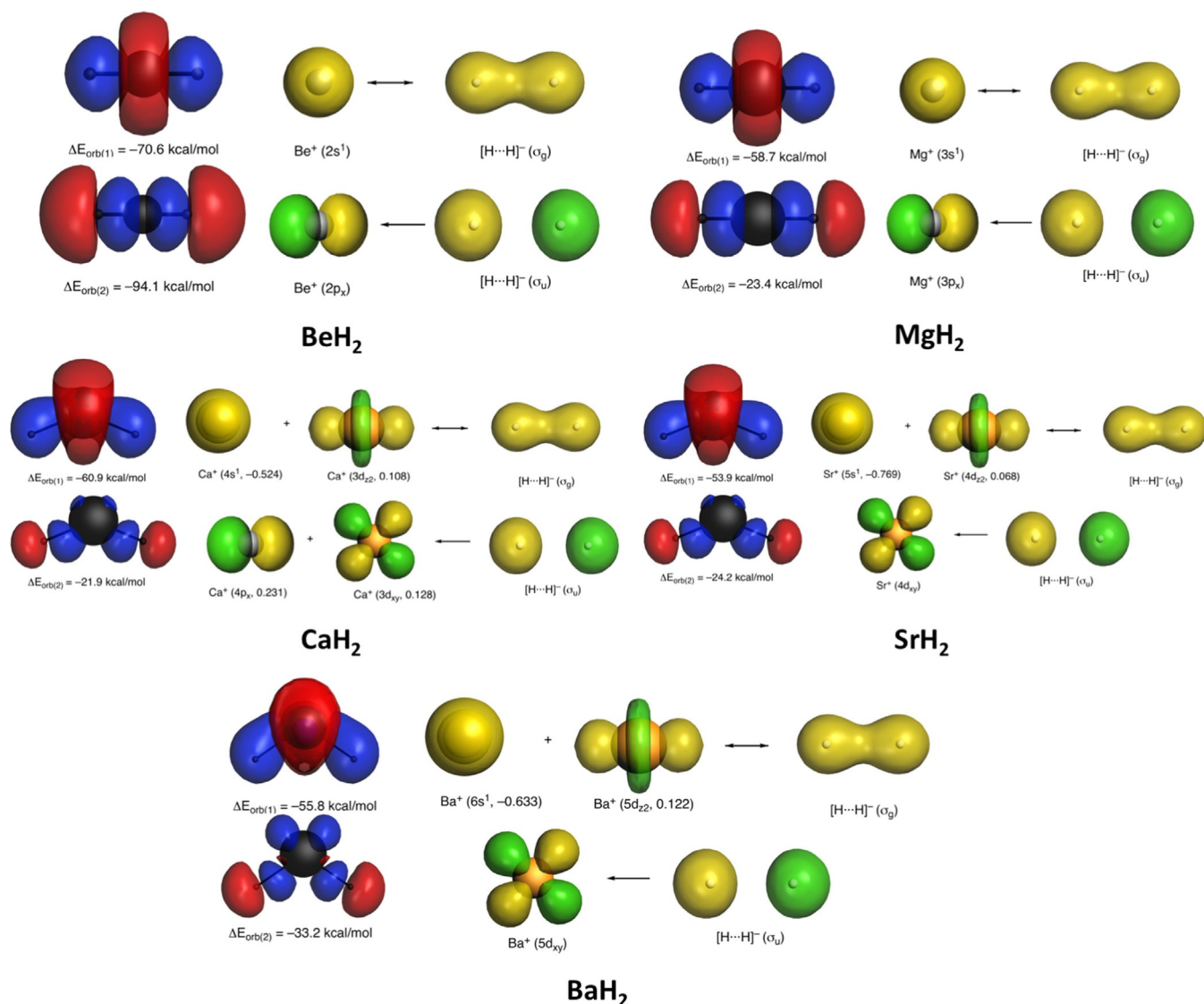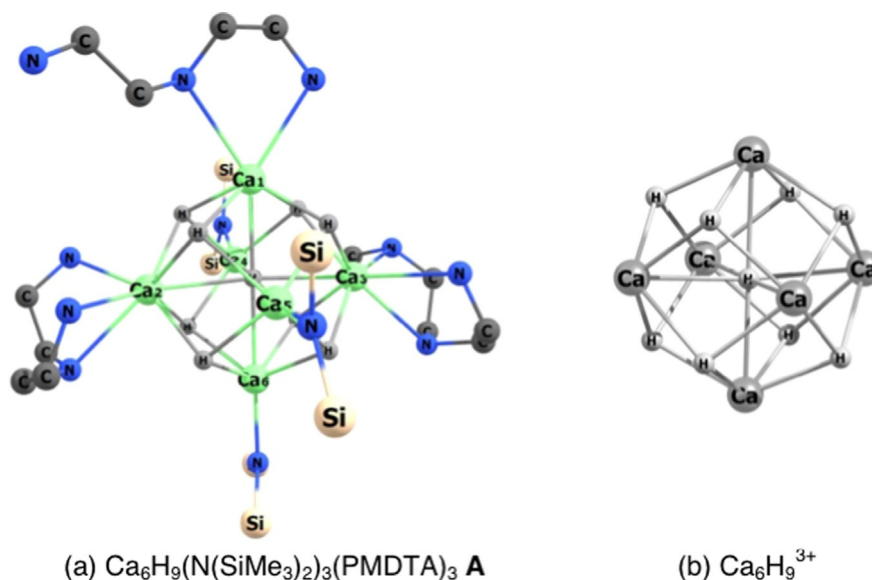**Chemistry**
Europe
European Chemical
Societies Publishing
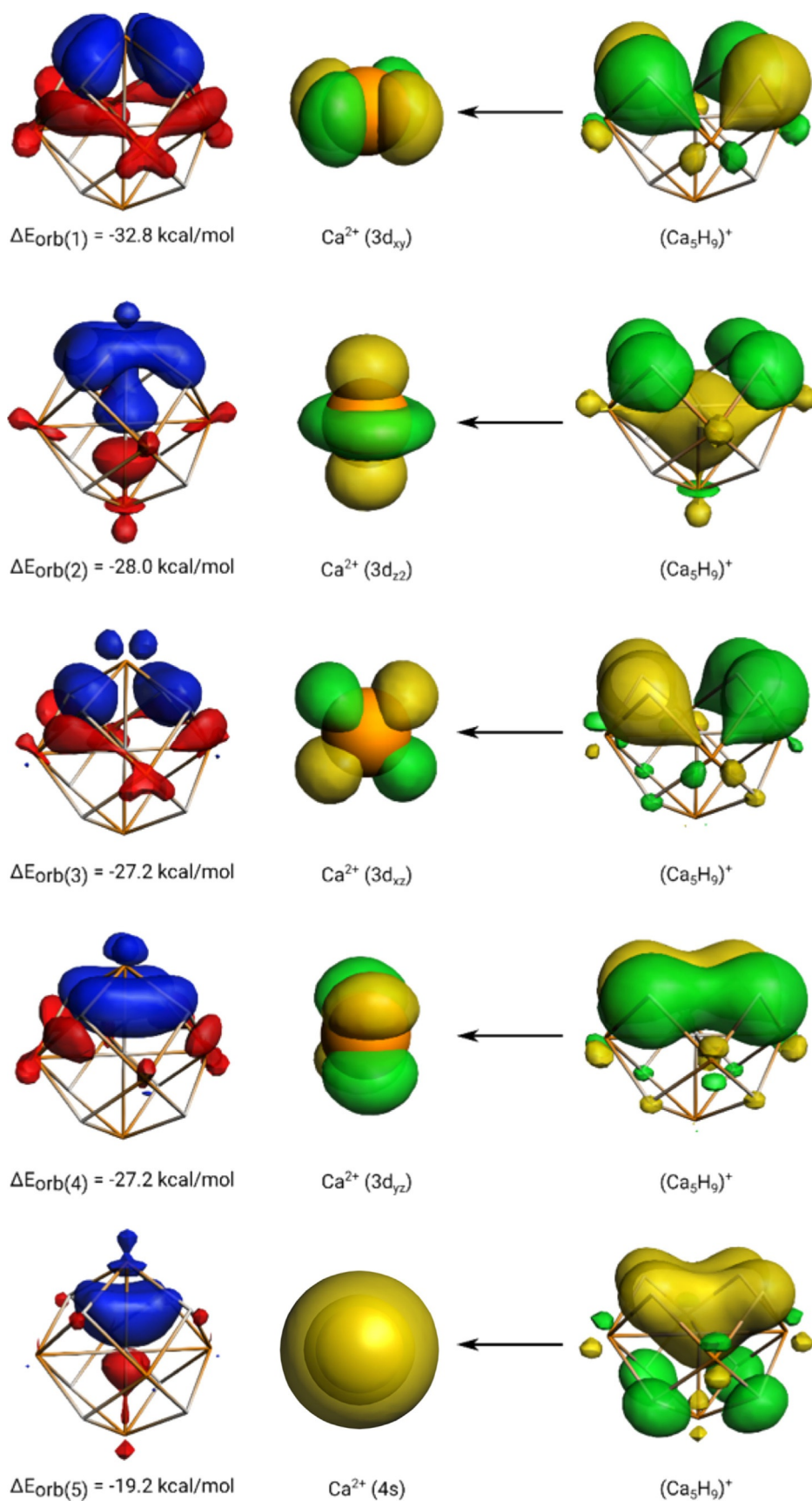
Figure 6. Deformation densities $\Delta\rho_1$–$\Delta\rho_5$ and the associated atomic orbitals of the most important orbital interactions $\Delta E_{orb(1)}$–$\Delta E_{orb(5)}$ of $(Ca_6H_9)^{3+}$ > 15 kcal mol^{-1} calculated by using the fragments Ca^{2+} and $(Ca_5H_9)^{+}$ (Table 7). The colour code used to represent the flow of charge is red→blue.

Chemistry–A European Journal

Full Paper
doi.org/10.1002/chem.202002986

Chemistry Europe
European Chemical
Societies Publishing

bond stabilisation is due to the Coulombic interaction of the accumulated charge in the neighbourhood of the nuclei. The situation changes gradually but the physical basis of the covalent bond formation, that is, the interference of the wave functions, remains the same if the bond is polar. The contribution of the electrostatic (Coulombic) interaction may become larger but the driving force for the bond formation is still the interference of the atomic wave functions. In contrast, ionic bonds form essentially as a result of Coulombic interactions between charged species with small valence–valence overlap. In the solid state, the overall stabilisation of an ionic compound requires the interaction of all particles, which can be expressed in terms of point charges and a Madelung factor. Thus, polar bonds such as those in AeO make a large electrostatic contribution to the covalent interaction, but should not be interpreted as due to an ionic type of bonding. The origin of the covalent and polar bonds is the interference of the electronic wave functions of the atoms. It is therefore of great interest to analyse the valence orbitals of both atoms to understand the basic features of the bond.

The results of this work are interesting not only from a theoretical point of view, but they also shed new light on recent experimental findings of surprising chemical reactions of compounds of the heavier alkaline-earth atoms. Harder and co-workers reported catalytic reactions and other chemical processes involving compounds of calcium, strontium and barium.[55a] The joint experimental/theoretical study of alkene hydrogenation catalysed by compounds of the alkaline-earth elements highlighted the complex **D3**, in which Ca is sandwiched between two aromatic rings (Figure 7), which closely resembles the metal–ligand bonds in the recently synthesised tribenzene adducts $Ae(Bz)_3$ featuring a transition-metal bonding scenario.[11] Harder and co-workers also reported the alkaline-earth-catalysed imine hydrogenation reaction.[55b] Okuda and co-workers introduced cationic calcium hydride catalysts for alkene hydrogenation.[56] The valence d orbitals of Ca may also play a role in the organocalcium-mediated nucleophilic alkylation of benzene recently reported by Wilson et al.[58] A very interesting study by Maron, Jones and co-workers revealed the kinetic stabilisation of a molecular strontium complex by a bulky amidinate ligand, showing surprising differences from a similar magnesium complex.[57] It may be worth examining the experimental findings for the structures and reactivities of compounds containing the heavier alkaline-earth metals in the light of the present findings, which point to chemical behaviour similar to that of early transition metals instead of main-group elements.

Summary and Conclusion

Analysis of the covalent bonds of the alkaline-earth metals Be, Mg, Ca, Sr and Ba in the oxides AeO, imides AeNH, dihydrides AeH_2 and the calcium cluster $Ca_6H_9[N(SiMe_3)_2]_3(pmdta)_3$ using charge and energy partitioning methods suggests that the valence orbitals of the lighter atoms Be and Mg are the $(n)s$ and $(n)p$ orbitals, whereas the valence orbitals of the heavier atoms Ca, Sr and Ba comprise the $(n)s$ and $(n-1)d$ orbitals. The alkaline-earth metals Be and Mg form covalent bonds like typical main-group elements, whereas Ca, Sr and Ba covalently bind like transition metals. The results not only shed new light on the covalent bonds of the heavier alkaline-earth metals, but are also very important for understanding and designing experimental studies.

Conflict of interest

The authors declare no conflict of interest.
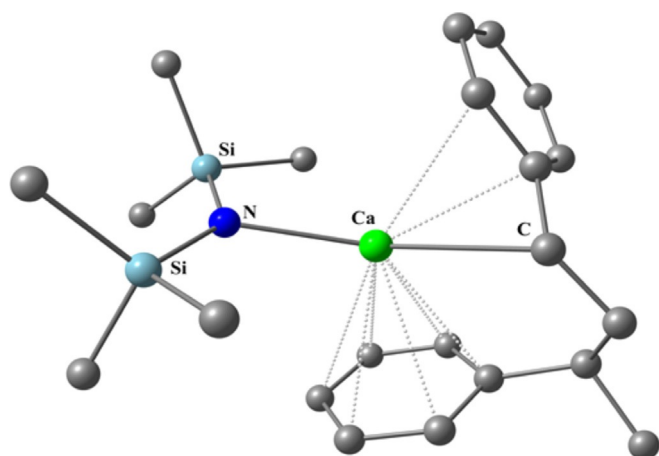
Figure 7. Calculated structure of compound **D3** with calcium sandwiched between two aromatic rings, which is relevant for the hydrogenation of alkenes catalysed by alkaline-earth atoms. The figure is adapted from reference [55a].

[1] a) M. Arrowsmith, H. Braunschweig, M. Celik, M. T. Dellermann, R. D. Dewhurst, W. C. Ewing, K. Hammond, T. Kramer, I. Krummenacher, J. Mies, K. Radacki, J. K. Schuster, *Nat. Chem.* **2016**, *8*, 890–894; b) S. P. Green, C. Jones, A. Stasch, *Science* **2007**, *318*, 1754; c) S. A. Couchman, N. Holzmann, G. Frenking, D. J. D. Wilson, J. L. Dutton, *J. Chem. Soc. Dalton Trans.* **2013**, *42*, 11375; d) J. L. Dutton, G. Frenking, *Angew. Chem. Int. Ed.* **2016**, *55*, 13380; *Angew. Chem.* **2016**, *128*, 13576; e) C. Jones, S. Bonyhady, N. Holzmann, G. Frenking, A. Stasch, *Inorg. Chem.* **2011**, *50*, 12315.

[2] a) Holleman–Wiberg, *Inorganic Chemistry* (Ed.: N. Wiberg), Academic Press, San Diego, **2001**; b) C. Housecraft, A. G. Sharpe, *Inorganic Chemistry*, 5th ed., Pearson, London, **2018**.

[3] *Pearson's Crystal Data*, ASM International, Materials Park (Eds.: P. Villars, K. Cenzual), Ohio, **2019**.

[4] *Constants of Diatomic Molecules* (Eds.: K. P. Huber, G. Herzberg), Springer, New York, **1979**.

[5] E. L. Burrows, S. F. A. Kettle, *J. Chem. Educ.* **1975**, *52*, 58.

[6] For electrostatic attraction in nonpolar covalent bonds, see: a) A. Kovács, C. Esterhuysen, G. Frenking, *Chem. Eur. J.* **2005**, *11*, 1813; b) A. Krapp, F. M. Bickelhaupt, G. Frenking, *Chem. Eur. J.* **2006**, *12*, 9196.

[7] L. Pauling, *The Nature of the Chemical Bond*, Cornell University Press, Ithaca, **1939**. The last (third) edition was published in 1960.

[8] X. Wu, L. Zhao, J. Jin, S. Pan, W. Li, X. Jin, G. Wang, M. Zhou, G. Frenking, *Science* **2018**, *361*, 912.

[9] Q. Wang, S. Pan, S. Lei, J. Jin, G. Deng, G. Wang, L. Zhao, M. Zhou, G. Frenking, *Nat. Commun.* **2019**, *10*, 3375.

[10] Q. Wang, S. Pan, Y. Wu, G. Deng, G. Wang, L. Zhao, M. Zhou, G. Frenking, *Angew. Chem. Int. Ed.* **2019**, *58*, 17365; *Angew. Chem.* **2019**, *131*, 17526.

[11] X. Wu, L. Zhao, D. D. Jiang, I. Fernandez, R. Berger, M. F. Zhou, G. Frenking, *Angew. Chem. Int. Ed.* **2018**, *57*, 3974–3980; *Angew. Chem.* **2018**, *130*, 4038–4044.

[12] C. R. Landis, R. P. Hughes, F. Weinhold, *Science* **2019**, *365*, eaay2355. For a reply see: L. Zhao, S. Pan, M. Zhou, G. Frenking, *Science* **2019**, *365*, eaay5021.

[13] a) J. F. van der Maelen, *Organometallics* **2020**, *39*, 132. b) For a comment, see: N. Holzmann, I. Fernández, G. Frenking, *Organometallics* **2020**, *39*, 2956.

[14] D. Koch, Y. Chen, P. Golub, S. Manzhos, *Phys. Chem. Chem. Phys.* **2019**, *21*, 20814.

[15] L. Gagliardi, P. Pyykkö, *Theor. Chem. Acc.* **2003**, *110*, 205.

[16] P. Pyykkö, *J. Chem. Soc. Faraday Trans.* **1979**, *75*, 1256.

[17] a) M. Kaupp in *The Chemical Bond. Chemical Bonding Across the Periodic Table* (Eds.: G. Frenking, S. Shaik), Wiley-VCH, Weinheim, **2014**, pp. 1–24; b) M. Kaupp, *Angew. Chem. Int. Ed.* **2001**, *40*, 3534; *Angew. Chem.* **2001**, *113*, 3642.

[18] A. Janczyk, D. L. Lichtenberger, L. M. Ziurys, *J. Am. Chem. Soc.* **2006**, *128*, 1109.

[19] H. Yu, D. G. Truhlar, *J. Chem. Theory Comput.* **2014**, *10*, 2291.

[20] C. R. Landis, F. Weinhold, *Valency and Bonding: A Natural Bond Orbital Donor-Acceptor Perspective*, Cambridge University Press, Cambridge, **2005**.

[21] a) A. Michalak, M. Mitoraj, T. Ziegler, *J. Phys. Chem. A* **2008**, *112*, 1933; b) M. P. Mitoraj, A. Michalak, T. Ziegler, *J. Chem. Theory Comput.* **2009**, *5*, 962.

[22] a) W. Heitler, F. London, *Z. Phys.* **1927**, *44*, 455; b) K. Ruedenberg, *Rev. Mod. Phys.* **1962**, *34*, 326; c) L. Zhao, W. H. E. Schwarz, G. Frenking, *Nat. Rev. Chem.* **2019**, *3*, 35; d) L. Zhao, S. Pan, N. Holzmann, P. Schwerdtfeger, G. Frenking, *Chem. Rev.* **2019**, *119*, 8781.

[23] a) P. Jerabek, P. Schwerdtfeger, G. Frenking, *J. Comput. Chem.* **2019**, *40*, 247; b) U. Pidun, G. Frenking, *Organometallics* **1995**, *14*, 5325; c) U. Pidun, G. Frenking, *J. Organomet. Chem.* **1996**, *525*, 269.

[24] a) U. Pidun, G. Frenking, *J. Chem. Soc. Dalton Trans.* **1997**, 1653; b) G. Frenking, N. Fröhlich, *Chem. Rev.* **2000**, *100*, 717.

[25] a) S. F. Vyboishchikov, G. Frenking, *Chem. Eur. J.* **1998**, *4*, 1428; b) S. F. Vyboishchikov, G. Frenking, *Chem. Eur. J.* **1998**, *4*, 1439.

[26] a) A. D. Becke, *Phys. Rev. A* **1988**, *38*, 3098; b) J. P. Perdew, *Phys. Rev. B* **1986**, *33*, 88224.

[27] a) F. Weigend, R. Ahlrichs, *Phys. Chem. Chem. Phys.* **2005**, *7*, 3297; b) F. Weigend, *Phys. Chem. Chem. Phys.* **2006**, *8*, 1057.

[28] P. Stegner, C. Färber, J. Oetzel, U. Siemeling, M. Wiesinger, J. Langer, S. Pan, N. Holzmann, G. Frenking, U. Abold, B. Sarkar, S. Harder, *Angew. Chem. Int. Ed.* **2020**, *59*, 14615; *Angew. Chem.* **2020**, *132*, 14723.

[29] Gaussian 16, Revision A.03, M. J. Frisch, G. W. Trucks, H. B. Schlegel, G. E. Scuseria, M. A. Robb, J. R. Cheeseman, G. Scalmani, V. Barone, G. A. Petersson, H. Nakatsuji, X. Li, M. Caricato, A. V. Marenich, J. Bloino, B. G. Janesko, R. Gomperts, B. Mennucci, H. P. Hratchian, J. V. Ortiz, A. F. Izmaylov, J. L. Sonnenberg, D. Williams-Young, F. Ding, F. Lipparini, F. Egidi, J. Goings, B. Peng, A. Petrone, T. Henderson, D. Ranasinghe, V. G. Zakrzewski, J. Gao, N. Rega, G. Zheng, W. Liang, M. Hada, M. Ehara, K. Toyota, R. Fukuda, J. Hasegawa, M. Ishida, T. Nakajima, Y. Honda, O. Kitao, H. Nakai, T. Vreven, K. Throssell, J. A. Montgomery, Jr., J. E. Peralta, F. Ogliaro, M. J. Bearpark, J. J. Heyd, E. N. Brothers, K. N. Kudin, V. N. Staroverov, T. A. Keith, R. Kobayashi, J. Normand, K. Raghavachari, A. P. Rendell, J. C. Burant, S. S. Iyengar, J. Tomasi, M. Cossi, J. M. Millam, M. Klene,

[30] C. Adamo, R. Cammi, J. W. Ochterski, R. L. Martin, K. Morokuma, O. Farkas, J. B. Foresman, D. J. Fox, Gaussian, Inc., Wallingford CT, **2016**.

[30] R. Ahlrichs, M. Bär, M. Häser, H. Horn, C. Kölmel, *Chem. Phys. Lett.* **1989**, *162*, 165.

[31] K. Eichkorn, O. Treutler, H. Öhm, M. Häser, R. Ahlrichs, *Chem. Phys. Lett.* **1995**, *242*, 652.

[32] a) B. Maitland, M. Wiesinger, J. Langer, G. Ballmann, J. Pahl, H. Elsen, C. Färber, S. Harder, *Angew. Chem. Int. Ed.* **2017**, *56*, 11880; *Angew. Chem.* **2017**, *129*, 12042; b) M. Wiesinger, B. Maitland, C. Färber, G. Ballmann, C. Fischer, H. Elsen, S. Harder, *Angew. Chem. Int. Ed.* **2017**, *56*, 16654; *Angew. Chem.* **2017**, *129*, 16881.

[33] E. D. Glendening, C. R. Landis, C. F. Weinhold, *J. Comput. Chem.* **2013**, *34*, 1429.

[34] T. Ziegler, A. Rauk, *Theor. Chim. Acta* **1977**, *46*, 1.

[35] a) M. Mitoraj, A. Michalak, *Organometallics* **2007**, *26*, 6576; b) M. Mitoraj, A. Michalak, *J. Mol. Model.* **2008**, *14*, 681.

[36] a) ADF2017, SCM, Theoretical Chemistry, Vrije Universiteit, Amsterdam, The Netherlands, http://www.scm.com; b) G. te Velde, F. M. Bickelhaupt, E. J. Baerends, C. F. Guerra, S. J. A. Van Gisbergen, J. G. Snijders, T. Ziegler, *J. Comput. Chem.* **2001**, *22*, 931.

[37] E. van Lenthe, E. J. Baerends, *J. Comput. Chem.* **2003**, *24*, 1142.

[38] E. van Lenthe, A. Ehlers, E. J. Baerends, *J. Chem. Phys.* **1999**, *110*, 8943.

[39] a) L. Zhao, M. von Hopffgarten, D. M. Andrada, G. Frenking, *WIREs Comput. Mol. Sci.* **2018**, *8*, e1345; b) G. Frenking, F. M. Bickelhaupt in *The Chemical Bond. Fundamental Aspects of Chemical Bonding* (Eds.: G. Frenking, S. Shaik), Wiley-VCH, Weinheim, **2014**, pp. 121–158; c) G. Frenking, R. Tonner, S. Klein, N. Takagi, T. Shimizu, A. Krapp, K. K. Pandey, P. Parameswaran, *Chem. Soc. Rev.* **2014**, *43*, 5106; d) L. Zhao, M. Hermann, N. Holzmann, G. Frenking, *Coord. Chem. Rev.* **2017**, *344*, 163; e) G. Frenking, M. Hermann, D. M. Andrada, N. Holzmann, *Chem. Soc. Rev.* **2016**, *45*, 1129; f) L. Zhao, M. Hermann, W. H. E. Schwarz, G. Frenking, *Nat. Rev. Chem.* **2019**, *3*, 48.

[40] M. A. Spackman, E. N. Maslen, *J. Phys. Chem.* **1986**, *90*, 2020.

[41] C. Chi, S. Pan, L. Meng, M. Luo, L. Zhao, M. Zhou, G. Frenking, *Angew. Chem. Int. Ed.* **2019**, *58*, 1732; *Angew. Chem.* **2019**, *131*, 1746.

[42] EDA-NOCV calculations were carried out on the singlet and triplet states for the neutral atomic fragments. For BeO, smaller values of ΔE_{orb} were obtained for the singlet state than for the triplet states, whereas for the heavier systems the triplet states were more favourable than the singlet states, but in all cases the numbers were much higher than when using charged fragments.

[43] a) Q. Zhang, W.-L. Li, C. Xu, M. Chen, M. Zhou, J. Li, D. M. Andrada, G. Frenking, *Angew. Chem. Int. Ed.* **2015**, *54*, 11078; *Angew. Chem.* **2015**, *127*, 11230; b) D. M. Andrada, G. Frenking, *Angew. Chem. Int. Ed.* **2015**, *54*, 12319; *Angew. Chem.* **2015**, *127*, 12494; c) C. Mohapatra, S. Kundu, A. N. Paesch, R. Herbst-Irmer, D. Stalke, D. M. Andrada, G. Frenking, H. W. Roesky, *J. Am. Chem. Soc.* **2016**, *138*, 10429; d) L. T. Scharf, M. Andrada, G. Frenking, V. H. Gessner, *Chem. Eur. J.* **2017**, *23*, 4422; e) M. Hermann, G. Frenking, *Chem. Eur. J.* **2017**, *23*, 3347; f) D. C. Georgiou, L. Zhao, D. J. D. Wilson, G. Frenking, J. L. Dutton, *Chem. Eur. J.* **2017**, *23*, 2926; g) Z. Wu, J. Xu, L. Sokolenko, Y. L. Yagupolskii, R. Feng, Q. Liu, Y. Lu, L. Zhao, I. Fernández, G. Frenking, T. Trabelsi, J. S. Francisco, X. Zeng, *Chem. Eur. J.* **2017**, *23*, 16566; h) W. Petz, D. M. Andrada, M. Hermann, G. Frenking, B. Neumüller, *Z. Anorg. Allg. Chem.* **2017**, *643*, 1096; i) D. M. Andrada, J. L. Casalz-Sainz, A. M. Pendás, G. Frenking, *Chem. Eur. J.* **2018**, *24*, 9083; j) R. Saha, S. Pan, G. Merino, P. K. Chattaraj, *Angew. Chem. Int. Ed.* **2019**, *58*, 8372; *Angew. Chem.* **2019**, *131*, 8460; k) T. Yang, D. M. Andrada, G. Frenking, *Mol. Phys.* **2019**, *117*, 1306.

[44] a) Z. L. Xiao, R. H. Hauge, J. L. Margrave, *High Temp. Sci.* **1991**, *31*, 59; b) Computational Chemistry Comparison and Benchmark DataBase, Release 20 (August 2019), National Institute of Standard and Technology.

[45] a) T. J. Tague, Jr., L. Andrews, *J. Am. Chem. Soc.* **1993**, *115*, 12111; b) T. J. Tague, Jr., L. Andrews, *J. Phys. Chem.* **1994**, *98*, 8611; c) X. Wang, L. Andrews, *J. Phys. Chem. A* **2004**, *108*, 11500.

[46] a) P. F. Bernath, A. Shayesteh, K. Tereszchuk, R. Colin, *Science* **2002**, *297*, 1323; b) A. Shayesteh, K. Tereszchuk, P. F. Bernath, R. Colin, *J. Chem. Phys.* **2003**, *118*, 3622; c) A. Shayesteh, D. R. T. Appadoo, I. Gordon, P. F. Bernath, *J. Chem. Phys.* **2003**, *119*, 7785; d) A. Shayesteh, K. A. Walker, I. Gordon, D. R. T. Appadoo, P. F. Bernath, *J. Mol. Struct.* **2004**, *695*, 23.

[47] R. L. De Kock, M. A. Peterson, L. K. Timmer, E. J. Baerends, P. Vernooijs, *Polyhedron* **1990**, *9*, 1919.

[48] a) M. Kaupp, P. v. R. Schleyer, H. Stoll, H. Preuss, *J. Chem. Phys.* **1991**, *94*, 1360; b) M. Kaupp, P. von R. Schleyer, H. Stoll, *J. Phys. Chem.* **1992**, *96*, 9801.

[49] I. Bytheway, R. J. Gillespie, T.-H. Tang, R. F. W. Bader, *Inorg. Chem.* **1995**, *34*, 2407.

[50] T. Shunmei Fujii, S. Iwata, *Chem. Phys. Lett.* **1996**, *251*, 150.

[51] G. S. Tschumper, H. F. Schaefer, *J. Chem. Phys.* **1998**, *108*, 7511.

[52] L. von Szentpály, *J. Phys. Chem. A* **2002**, *106*, 11945.

[53] H. Li, D. Xiea, H. Guo, *J. Chem. Phys.* **2004**, *121*, 4156.

[54] J. Koput, *J. Phys. Chem. A* **2005**, *109*, 4410.

[55] a) H. Bauer, M. Alonso, C. Fischer, B. Rösch, H. Elsen, S. Harder, *Angew. Chem. Int. Ed.* **2018**, *57*, 15177; *Angew. Chem.* **2018**, *130*, 15397; b) H. Bauer, M. Alonso, C. Färber, H. Elsen, J. Pahl, A. Causero, G. Ballmann, F. De Proft, S. J. Harder, *Nat. Catal.* **2018**, *1*, 40; c) T. X. Gentner, B. Rösch, K. Thum, J. Langer, G. Ballmann, J. Pahl, W. A. Donaubauer, F. Hampel, S. Harder, *Organometallics* **2019**, *38*, 2485.

[56] a) P. Jochmann, J. P. Davin, T. P. Spaniol, L. Maron, J. Okuda, *Angew. Chem. Int. Ed.* **2012**, *51*, 4452; *Angew. Chem.* **2012**, *124*, 4528; b) V. Leich, T. P. Spaniol, L. Maron, J. Okuda, *Angew. Chem. Int. Ed.* **2016**, *55*, 4794; *Angew. Chem.* **2016**, *128*, 4872; c) D. Schuhknecht, C. Lhotzky, T. P. Spaniol, L. Maron, J. Okuda, *Angew. Chem. Int. Ed.* **2017**, *56*, 12367; *Angew. Chem.* **2017**, *129*, 12539.

[57] A. S. S. Wilson, M. S. Hill, M. F. Mahon, C. Dinoi, L. Maron, *Science* **2017**, *358*, 1168.

[58] C. N. de Bruin-Dickason, T. Sutcliffe, C. A. Lamsfus, G. B. Deacon, L. Maron, C. Jones, *Chem. Commun.* **2018**, *54*, 786.

[59] A. Kramida, Yu. Ralchenko, J. Reader, and NIST ASD Team (2019). *NIST Atomic Spectra Database* (ver. 5.7.1), [Online]. Available: https://physics.-nist.gov/asd [2020, March 18]. National Institute of Standards and Technology, Gaithersburg, MD. https://doi.org/10.18434/T4W30F.

[60] a) G. B. Bacskay, S. Nordholm, K. Ruedenberg, *J. Phys. Chem. A* **2018**, *122*, 7880; b) A. C. West, M. W. Schmidt, M. S. Gordon, K. Ruedenberg, *J. Phys. Chem. A* **2017**, *121*, 1086; c) T. Bitter, K. Ruedenberg, W. H. E. Schwarz, *J. Comput. Chem.* **2007**, *28*, 411; d) T. Bitter, S. G. Wang, K. Ruedenberg, W. H. E. Schwarz, *Theor. Chem. Acc.* **2010**, *127*, 237; e) M. W. Schmidt, J. Ivanic, K. Ruedenberg in *The Chemical Bond. 1. Fundamental Aspects of Chemical Bonding* (Eds.: G. Frenking, S. Shaik), Wiley-VCH, Weinheim, **2014**, p. 1–67; f) W. Kutzelnigg, *Angew. Chem. Int. Ed. Engl.* **1973**, *12*, 546; *Angew. Chem.* **1973**, *85*, 551.